Plasma cryogenic etching of silicon: from the early days to today's advanced technologies

2014 J. Phys. D: Appl. Phys. 47 123001

(http://iopscience.iop.org/0022-3727/47/12/123001)

IOP Publishing Journal of Physics D: Applied Physics
J. Phys. D: Appl. Phys. **47** (2014) 123001 (27pp) doi:10.1088/0022-3727/47/12/123001

Topical Review

Plasma cryogenic etching of silicon: from the early days to today's advanced technologies

R Dussart[1], T Tillocher[1], P Lefaucheux[1] and M Boufnichel[2]

[1] GREMI, CNRS/Université d'Orléans, 14 rue d'Issoudun, BP 6744, F-45067 Orléans, France
[2] STMicroelectronics, 16 rue Pierre et Marie Curie, BP 7155, F-37071 Tours, France

E-mail: remi.dussart@univ-orleans.fr

Received 29 November 2013, revised 22 January 2014
Accepted for publication 23 January 2014
Published 6 March 2014

Abstract

The evolution of silicon cryoetching is reported in this topical review, from its very first introduction by a Japanese team to today's advanced technologies. The main advances in terms of the performance and comprehension of the mechanisms are chronologically presented. After presenting the principle of silicon cryoetching, the main defects encountered in cryoetching (such as undercut, bowing and crystal orientation dependent etching) are presented and discussed. Mechanisms involved in SiO_xF_y passivation layer growth in standard cryoetching are investigated through several *in situ* characterization experiments. The STiGer process and alternative cryoetching processes for high-aspect-ratio structures are also proposed to enhance the process robustness. The over-passivation regime, which can provide self-organized columnar microstructures, is presented and discussed. Finally, advanced technologies, such as the cryoetching of sub-20 nm features and porous OSG low-*k* cryoetching, are described.

Keywords: cryoetching, cryogenic etching, black silicon, silicon deep etching, low-*k*

(Some figures may appear in colour only in the online journal)

1. Introduction

The deep etching of silicon has become an essential and critical step for many microelectronic components and MEMS demonstrators. Although silicon etching has been studied for more than 30 years, it remains an actual concern, especially in order to increase microdevice performance, to control critical dimensions, and to create new and original microstructures. More recently, silicon deep etching was needed for through silicon vias (TSV) and 3D microelectronic components in the 'More than Moore' trend [1].

Low pressure plasmas have been intensively used for deep etching since they offer many advantages compared to wet processes. Ion directivity due to the plasma sheath above the substrate can force the etching along the vertical direction and appears to be a good way to form high-aspect-ratio structures. However, ions are not always sufficient to achieve deep etching, especially when very reactive species are produced in the plasma and react spontaneously with the material to be etched, which leads to more or less isotropic profiles. This is the reason why additional gases are commonly used to create a passivation layer on the vertical sidewalls in order to prevent their erosion by spontaneous chemical reactions. Usually, process engineers have to tune process parameters to balance etching and passivation in order to obtain the wanted microstructure with limited defects. Among these defects, undercut, bowing, notching, trenching, micromasking are always irreversible, but they can be avoided by optimizing some of the process parameters. To be industrially used, an etching process has to be fast, robust, reproducible and as clean

as possible, not only in terms of reactor contamination but also in terms of environment protection.

For silicon high-aspect-ratio structures, two different processes are usually used, which are cryogenic processes and the so-called 'Bosch' process. Etching of very low-temperature silicon substrates was first introduced at the end of the 1980s [2]. About eight years later, the Bosch process was patented [3]. Because the Bosch process is quite robust and operates at ambient temperature (and has no need of liquid nitrogen), it has been preferred for industrial applications. However, this process also presents some drawbacks compared to the cryogenic process, which, can in turn appear as a good alternative for some particular devices.

Although the next section starts with a synthesized history of cryogenic etching, the reader can skip this part and start with the principle of the cryogenic etching of silicon in the second part of this section. Then, the advantages and drawbacks of cryoetching will be discussed in detail and a comparison will be made with the alternative processes for silicon deep etching. An overview of the passivation mechanisms involved in the cryoetching process will be presented in section 3. The so-called STiGer process and other cyclic process will be discussed in section 4. Then, in section 5, black silicon and silicon columnar microstructures (CMSs) formed in the over-passivating regime will be detailed. Finally, new challenges of cryoetching and advanced cryoetching processes for low-k materials will be discussed in section 6 and the last section.

2. State of the art of cryoetching technology

2.1. History of cryoetching

Cryogenic etching of silicon was first introduced by Tachi *et al* in 1988 [2]. At that time, it was difficult to obtain anisotropy, high etch rate, and high selectivity at once. Although a high etch rate could be achieved with SF_6 plasmas, anisotropic etching was not possible with this gas and usually deep anisotropic plasma etching was carried out with other gas mixtures, such as CF_4/O_2 [4], SF_6/CHF_3 [5], or with gases containing other halogen atoms, such as Br [6]. Tachi's team proposed to cool the substrate down to a temperature between -100 and $-130\,^{\circ}C$ while running a microwave SF_6 plasma. The electrode holding the substrate could be biased independently by RF excitation. The idea was to freeze chemical reactions on vertical sidewalls of the sample and favour ion-assisted reactions at the feature bottom. Samples were covered either by a photoresist (AZ1350J) mask or by a SiO_2 layer. The authors compared the obtained profile of 0.8 μm wide trenches versus temperature in the following two different configurations: in the capacitively coupled plasma (CCP) configuration and in a microwave plasma reactor. In both cases, they obtained anisotropic profiles only at low temperature (below $-70\,^{\circ}C$). As mentioned in the same paper, below $-140\,^{\circ}C$ no etching was observed because the SF_6 started to condense on cold surfaces. Their results are summarized in figure 1, where etch rates of silicon and photoresist are shown versus temperature. The normalized side etch width R is also plotted (right y-axis). An etch depth

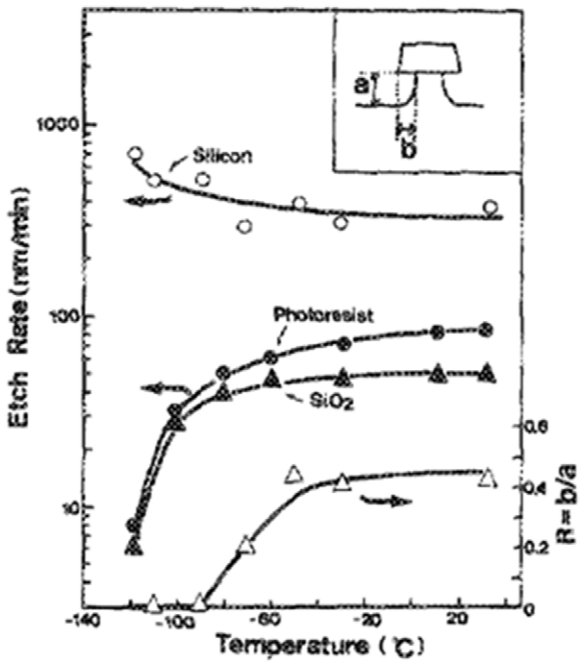

Figure 1. Temperature dependence of etch rates of Si, the photoresist, and SiO_2, and the normalized side etch width R, which is defined as $R =$ (side etch width/etch depth). Reproduced with permission from [2]. Copyright 1988 American Institute of Physics.

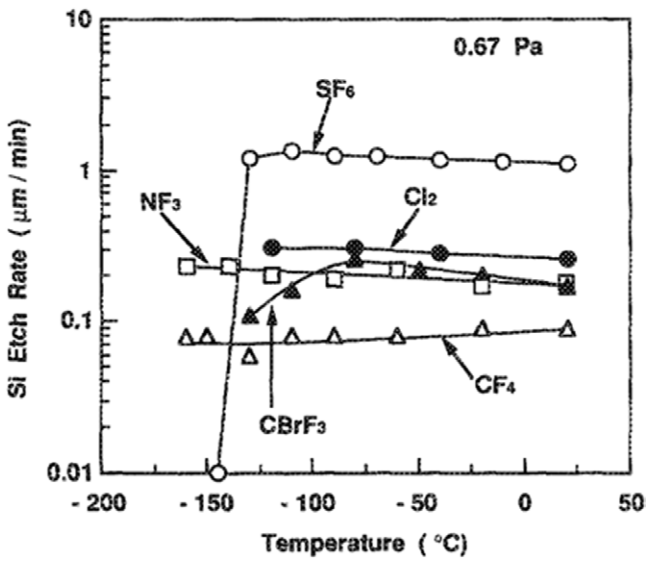

Figure 2. Silicon etch rates for SF_6, CF_4, NF_3, Cl_2, $CBrF_3$, gas plasmas measured as a function of wafer temperature. Reproduced with permission from [7]. Copyright 1991 American Institute of Physics.

of the order of 1 μm was achieved, which cannot be considered as deep etching, but the proof of principle of cryogenic etching was shown and the effect of temperature was evidenced.

In 1991, the same team published a study of the interaction between ions and the low-temperature silicon surface [7]. They also investigated different gases (SF_6, Cl_2, HBr, etc) and other materials (W, SiO_2, Al, etc) at low temperatures. It is clear from figure 2 that the SF_6 gas was giving the highest etch rates. It is also interesting to observe from this figure that the etch rate remains more or less constant versus temperature.

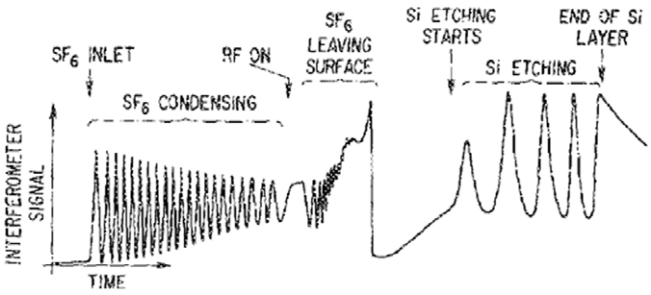

Figure 3. Laser interferometry signal as a function of time during a low-temperature experiment. Reproduced with permission from [8]. Copyright 1990 American Institute of Physics.

Note that, in this paper, a cyclic process to favour etching and deposition in order to protect sidewalls had been proposed for the first time (the authors gave an example by alternating fluoride and chloride gases). The authors provided the system requirements to compensate the heat during etching due to both plasma species energy transfer and etching reactions at the surface. They also observed a reduction of the undercut below $-60\,^{\circ}$C when etching silicon with Cl_2. In general, the authors explained the phenomenon by a low reaction probability of the radicals at very low temperature.

In 1990, a paper was published by Bestwick *et al* on cryogenic reactive ion etching of silicon in SF_6 [8]. A CCP reactor was used and the powered electrode was cooled at liquid-nitrogen temperature. The authors used laser interferometry to identify three regimes: SF_6 condensation, SF_6 desorption, and silicon etching (figure 3).

They also made some characterization by mass spectrometry and by optical emission spectroscopy (OES). In their experiment, the authors used patterned wafers with SiO_2 mask and polycrystalline silicon over oxide on a silicon substrate. The selectivity was found to be lower than at ambient temperature. They also found a higher self-bias at low temperature. F_2 species were identified from optical emission spectra only at low temperature, which came (according to the authors) from the recombination of F–F atoms during the removal of SF_x species from the gas phase by condensation. At the end of their paper, they concluded that although this liquid-nitrogen temperature revealed interesting phenomena, the temperature regime down to $-140\,^{\circ}$C was technologically more useful.

From an additional paper from the Japanese team mentioned earlier [9], we learn that the 260 mm diameter discharge tube was made of fused silica. They presented P-type crystalline silicon (1 0 0) etching performances by using several gases (SF_6, CF_4, NF_3) with two different masks (AZ1350J and SiO_2). In their experimental conditions, an etch rate of 1 μm min^{-1} was reached for a process duration of 5 min. A study was performed versus pressure and temperature. An aspect ratio of as high as 5 was obtained for the first time using the cryogenic etching process.

In 1993, Aydil *et al* designed and characterized an ECR reactor to etch compound semiconductors and Si at low temperatures [10].

In 1995, Bartha *et al* [11] performed some silicon cryogenic etching experiments using both a distributed electron cyclotron resonance (DECR) system and a helicon type plasma reactor. In their experiments, they did not obtain anisotropic etch profiles in pure SF_6 plasma, even at temperatures below $-120\,^{\circ}$C. They needed to add O_2 to obtain anisotropic etch profiles. They also obtained a quite high etch rate (5 μm min^{-1}) and a very good selectivity above (100 : 1) with SiO_2 masks. For the first time, a mechanism based on sidewall passivation was suggested in cryogenic etching instead of a mechanism based on a low reaction probability of the radicals on very cold silicon surfaces. According to the authors, the anisotropic profiles obtained by the Japanese team was partly due to the oxygen released from fused silica in contact with the SF_6 plasma, whose equivalent flow was estimated to be several sccm in such an experiment. This non-negligible O_2 flow could be responsible for the anisotropic etching obtained in the first cryogenic etching experiments reported by Tachi *et al* [2]. The plasma reactors used by Bartha did not contain such an O_2 contamination source. Above a certain amount of O_2 flow, black silicon appeared at the surface. They concluded that O_2 addition was a very sensitive control parameter to form anisotropic etched profiles and advised to avoid quartz in contact with the plasma to eliminate an oxygen source that could modify the process. Very promising results were obtained by the same team in a helicon plasma source [12]. Such a helicon plasma source had been introduced earlier for silicon etching by Boswell *et al* [13, 14].

This was not the first time that O_2 had been added to SF_6 plasma for silicon etching at ambient temperature: d'Agostino *et al* studied this chemistry and the species formed in this type of plasma mixture, especially to give an alternative to CF_4/O_2 plasmas that were used for silicon etching at the end of the 1970s [15]. The remaining oxide layer formed on the sidewalls at ambient temperature in SF_6/O_2 plasma was analysed by x-ray photoelectron spectroscopy (XPS) [16].

In 1995, Jansen *et al* started a series of articles on the so-called 'black-silicon method' for silicon deep etching. The technique is based on the appearance of black silicon in SF_6/O_2 plasma. The authors suggest to add CHF_3 to scavenge O atoms and leave the black-silicon regime, and then create a more efficient passivation layer to protect the sidewall [17–19].

Another Japanese team published results very close to those obtained by Tachi, but using a CCP reactor equipped with a permanent magnet to enhance the plasma density [20]. They worked with a quite low flow of SF_6 (2.5–5 sccm). They were also able to etch silicon anisotropically without adding oxygen in the plasma. These results are in contradiction to the results obtained by Bartha *et al*. However, the reactor material is not mentioned in detail, so it is difficult to know if this result is due to an unwanted source of oxygen in the reactor. At this low SF_6 pressure, a very small oxygen content can play an important role in the passivation. Very similar results were obtained by Wells *et al* [21]. Again, the authors obtained the best results at a very low flow of SF_6 (1 sccm). They also reported on a faceting effect that was attributed to oxygen, which could be provided by the feed gas or desorption from the wall. This low oxygen contamination could also be responsible for the anisotropic etching obtained at low temperature. However, this was the first time that crystal orientation dependent etching (CODE) in a cryogenic process had been reported.

The Bosch process, which consists of alternating isotropic etching (SF_6 plasma) and deposition steps (C_4F_8 plasma) to form high-aspect-ratio silicon profiles at ambient temperature, was patented in 1996 [3].

In 1997, Chevolleau *et al* reported on reactive ion beam etching (RIBE) of silicon at low temperature using SF_6 [22]. They studied the etch yield versus beam energy and evaluated the reaction probability of neutral fluorine atoms. They also made an XPS study of the silicon surface after process [23]. The surface was maintained at low temperature during the analysis. Although they did not observe any adsorption of SF_6, even at $-150\,^{\circ}C$, they evidenced an adsorbed layer mainly composed of SF_4 and SF_2 that was formed without ion bombardment. The layer thickness could be reduced when submitted to ion bombardment.

In 1998, a general review paper was published on sidewall surface chemistry in etching processes, in which low-temperature etching is discussed [24].

In 1999, Aachboun and Ranson published the first cryogenic etching tests performed at the GREMI lab. They were able to etch 80 μm deep, 2 μm wide trenches. Some bowing and undercut were observed at the top of the trenches. They also obtained a very high selectivity, greater than (500 : 1) using a SiO_2 mask [25]. One year later, they obtained better profiles with the same type of process and they estimated the etching uniformity on a 5 inch substrate. The wafer deformation due to the helium pressure at the backside was responsible for temperature gradients, which led to the rather bad uniformity [26].

In 1999, Zijlstra *et al* used the cryogenic etching to form a two-dimensional photonic band gap structure in silicon in order to meet the severe nanotolerance requirements [27]. They performed a parametric study of cryoetching as function of bias, oxygen content and temperature. In particular, they found that, beyond a certain value, increasing bias does not increase the etch rate but leads to negative slopes. They also reported on a CODE effect, as observed earlier by Wells *et al* [21]. A more detailed study of the crystallographic effect in the cryogenic process was published by the same team [28]. In the same paper, they also reported on the aspect ratio dependent etching (ARDE) in SF_6/O_2 cryogenic etching. In small features, Knudsen transport was found to be the main mechanism, which explains the ARDE observed in cryoetching. An etch rate as high as 11.5 μm min^{-1} was reported.

In 2001, Jansen *et al* published a new article dealing with the black-silicon method adapted to cryogenic etching [29]. In a diagram showing the oxygen content and the substrate temperature, a region of black-silicon appearance is clearly evidenced (see figure 4). Black silicon corresponds to a very rough surface of silicon, which appears black when enlightened. The suggested method consists in defining the black-silicon region using a dummy silicon wafer and then in working in conditions very close to the boundary between etching and black-silicon formation. Interestingly, this boundary is not a straight line and there is a temperature for which it is easier to form black silicon.

As reported, after optimization, an initial etch rate as high as 15 μm min^{-1} was achieved with a selectivity of the order of 2000 with SiO_2 or ordinary photoresist masks.

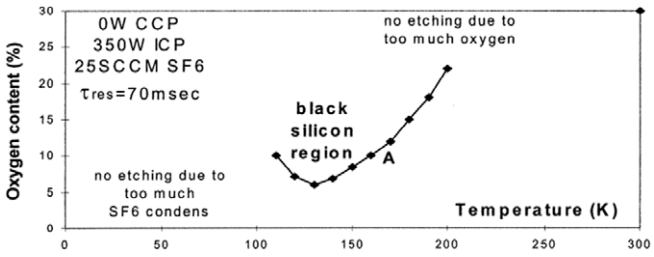

Figure 4. Black-silicon appearance conditions as a function of temperature and oxygen content. Reproduced with permission from [29]. Copyright 2001 Elsevier.

Finally, the main results on silicon cryoetching from 2002 to 2013 are summarized in table 1.

2.2. Basic principles involved in the cryoetching process

Although cryoetching can be performed in a CCP reactor [2, 20], high-density reactors such as inductively coupled plasma (ICP) are usually used for deep etching to control ion flux and ion energy independently and increase the etch rate. In cryoetching especially, a quite low self-bias (few tens of volts) is usually set [56] whereas a quite high power is injected into the source to create a high-density plasma and a high density of etching species. The scheme of such a reactor is shown in figure 5. The antenna is separated from the plasma by a tube, which can be made of quartz or alumina. Note that alumina is less etched than the quartz so that the tube does not need to be replaced often and less oxygen is released into the plasma. Usually, SF_6 and O_2 gases are injected into the source part of the reactor. As already mentioned, SF_6 is the gas that provides the most fluorine radicals and the highest etch rates are obtained with SF_6 plasmas (see figure 5) [2]. Oxygen flow corresponding to a proportion of typically 10% of the mixture is necessary to create the passivation layer at low temperature [28]. The RF antenna of the source can be surrounded by a confinement coil. At high density and low pressure, whistler plasma (helicon) waves can be launched and can provide an even higher plasma density [13]. The wafer is placed on a substrate holder in the diffusion chamber situated in the lower part of the reactor. Although different mask materials can be used, SiO_2 masks are usually preferred because of their very high selectivity and low contamination. The chuck is cooled with liquid nitrogen. Its temperature is measured and regulated by a proportional–integral–derivative (PID) controlled heating element, which allows the temperature to be set to a desired value, typically $-100\,^{\circ}C$. Note that the set-point temperature is usually measured inside the chuck and is not exactly the wafer temperature [62]. The substrate is biased by an independent RF power supply. Helium is injected between the substrate and the chuck to increase the thermal conductivity and favour heat evacuation, from both the plasma and the chemical reactions to the cooling system.

A scheme of the chemical and physical mechanisms involved in silicon cryoetching is represented in figure 6. Fluorine, SF_x and O radicals are created in the plasma source and diffuse towards the substrate. Fluorine radicals react spontaneously with silicon atoms and form SiF_x molecules

Table 1. Summary of the main published results in cryoetching between 2002 and 2013.

Year	Authors	Summary	References
2002	de Boer *et al*	Guidelines for the cryoetching of different MEMS structures using the 'black-silicon method'.	[30]
2002–2005	Boufnichel *et al*	Defects appearing in silicon cryoetching and how to reduce or eliminate them: local bowing formation and undercut.	[31–33]
		Simulation	
2003–2004	Marcos, Blauw *et al*	Silicon etching in SF_6/O_2 plasma at ambient and cryogenic temperatures by Monte Carlo simulation.	[34–36]
2002–2006	Kokkoris *et al*	ARDE effect.	[37]
		Desorption activation energy for SiF_4 molecule.	
		Anisotropic etching at very low pressure using a CCP reactor.	[38, 40]
	Knizikevicius	Etching anisotropy increase in SF_6/O_2 plasma due to the decreased desorption of formed SiF_4 molecules from the sidewalls at low temperature.	
2010	Maruyama	Monte Carlo simulations in SF_6/O_2 at ambient temperature. Knudsen transport model provides a remarkably good fit for experimental results on ARDE as reported earlier by Blauw *et al* [28].	[41]
2003	Rangelow	Review article on high-aspect-ratio silicon dry etching for MEMS.	[42]
2004–2009	GREMI's Team	Passivation mechanisms involved in the cryoetching process (detailed in section 3).	[43–49]
2007	Sainiemi and Franssila	Behaviour of eight different mask materials (different resists, alumina, SiO_2) in silicon cryoetching.	[49]
2007	Pruessner *et al*	Two step cryoetching process to form high-aspect-ratio submicrometre silicon trenches.	[50]
2008	Tillocher *et al*	STiGer process.	[51, 52]
2008	Isakovic *et al*	A cyclic cryogenic anisotropic plasma etching.	[53]
2009	Jansen *et al*	Review article on deep etching based on black-silicon method.	[54]
2009	Henry *et al*	Cryogenic etching process performances to create different sensors geometries.	[55]
2010	Sokmen *et al*	Submicrometre pores (300 nm diameter) and submicrometre diameter pillars using a standard cryoetching of silicon.	[56]
2010	Kamto *et al*	Fabrication of tapered TSV by cryoetching.	[57]
2011 2013	Wu *et al* Liu *et al*	Silicon cryoetching of nanometric features.	[58, 59]
2013	Zhang *et al*	Cryoetching of porous SiOCH low-*k* material.	[60, 61]

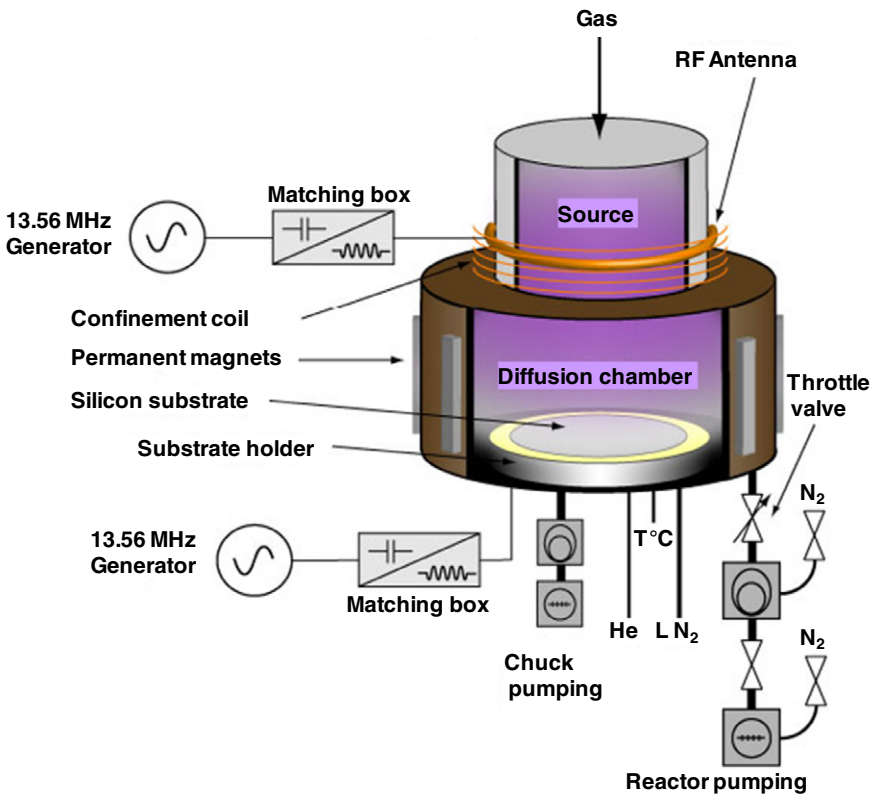

Figure 5. Scheme of a typical ICP reactor dedicated to cryoetching.

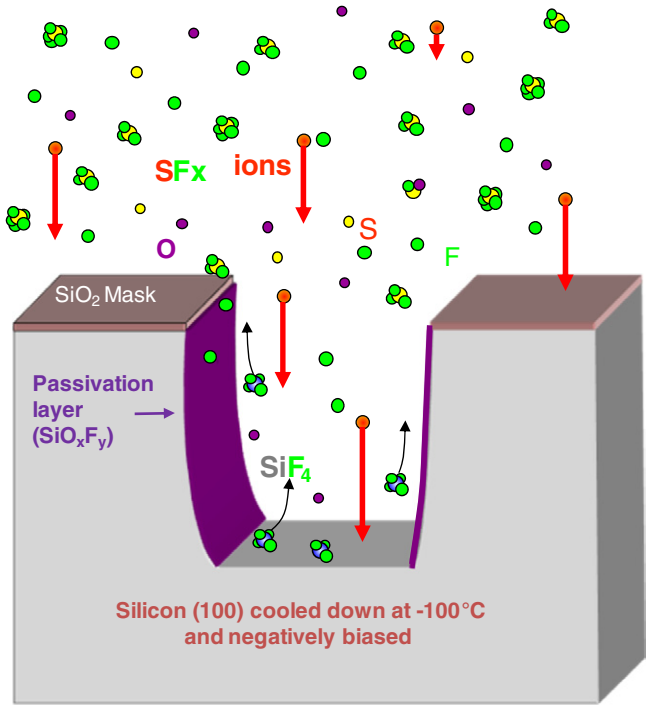

Figure 6. Scheme of principle of physical and chemical mechanisms involved in cryoetching.

at the surface. Without bias, fluorine can diffuse through about 2–5 monolayers before reacting with silicon [63]. SiF_4 is created via a very exothermal chemical reaction and then desorbs from the surface. SiF_4 is a very volatile product: its melting point temperature is −86.8 °C at atmospheric pressure. It is then either dissociated in the plasma or evacuated by the pumping system. Note that, although SiF_4 is the main by-product, other molecules such as SiF_2, Si_2F_6 or Si_3F_8 can be produced in a much lower proportion [63]. However, oxygen can interact with SiF_x and SiO_xF_y molecules are created, which subsequently block the etching mechanism. This siliconoxyhalide passivation layer forms on the vertical sidewalls where ions have a grazing incidence. At the trench bottom, the passivation layer does not form or is removed by the incident ion bombardment.

As will be explained in section 3, this passivation layer is very fragile. At ambient temperature, a SiO_xF_y passivation layer with a higher oxygen content also forms and is less fragile, but the etch rate is lower, selectivity with SiO_2 is weaker, and an undercut is still obtained [64]. To increase performances of these ambient temperature processes, some additional gases such as HBr can be used, particularly to reduce undercut [65].

Scanning electron microscopy (SEM) pictures of typical high-aspect-ratio trenches obtained with the standard cryogenic etching are shown in figure 7. The etch rate was 4 μm min^{-1} for 4 μm wide trenches (figure 7(*a*)). 1 μm wide and 31 μm deep trenches have also been etched using such a process at a rate of 2.6 μm min^{-1} (figure 7(*b*)). In the SEM image, the (1 1 1) plane can be observed at the trench bottom, which indicates a crystallographic effect during the etching process.

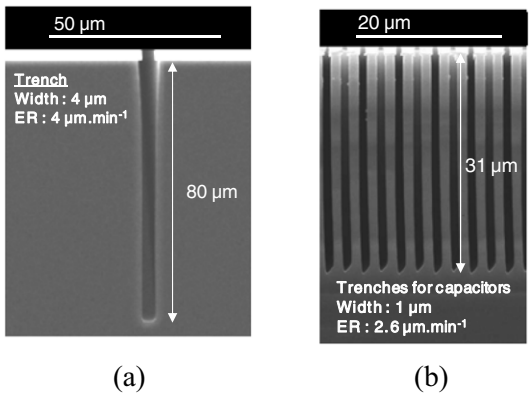

Figure 7. Typical trench profiles obtained in silicon cryoetching.

2.3. Advantages and limitations compared to alternative processes

A comparison of Bosch and cryogenic processes was published by Walker in 2001 [66]. First, silicon cryoetching process is clean compared to the Bosch process: no deposition occurs at the reactor walls since they are not cooled, so that it is not necessary to insert cleaning steps between processed wafers. In the Bosch process, C_4F_8 plasma steps induce CF_x deposition everywhere, including on the reactor walls. Cleaning steps are required, which reduces the production yield in terms of number of etched wafers per hour. As will be described in section 3, we showed that after cryoetching the profiles are clean and are not covered by the passivation layer as soon as they are warmed back to the ambient temperature. This is also an advantage for some microdevices.

The standard cryogenic etching of silicon is a one-step process: no alternations are needed. Consequently, no scalloping effect is obtained, which is an advantage for some microsystems containing micro-mirrors, for example.

Although the gases that are used are not hazardous, the main etching products (SiF_4) are. In addition, the Bosch process requires high flows of C_4F_8, which is a quite an expensive gas.

Until now, liquid nitrogen has been required for the cryoetching process. As already mentioned, a typical temperature of −100 °C is necessary to process wafers. Actual chillers cannot reach this very low temperature.

ARDE can be quite significant in cryoetching. As already mentioned, Blauw *et al* showed that ARDE was due to Knudsen transport of fluorine radicals [28]. In the Bosch process, this effect can be balanced by the deposition steps that tend to reverse ARDE, so that the global effect can be reduced.

Finally, although there is nearly no process drift in cryoetching, this type of process is very sensitive to certain parameters, such as O_2 flow and temperature. A shift of a few degrees can modify the profile slopes, which means that the wafer surface temperature must be as uniform as possible. A dedicated chuck achieving a very good temperature uniformity is sometimes necessary. In some cases, especially at high etch rate and for very deep etching, cryoetching processes are not robust enough. At high etch rates, the amount of energy due to the strong exothermal chemical reaction is significant [67]

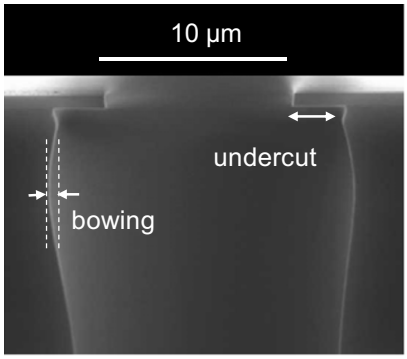

Figure 8. Example of bowing and undercut defects obtained after a cryoetching process.

and can be an issue for the control of the passivation layer. Moreover, according to the black-silicon method [29], one has to work very close to the black-silicon region to get the best performance. So, in the case of a small drift of the oxygen flow, micrograss can appear and etching ceases.

But, if the etching requirements are not too challenging in terms of etch rate, depth and aspect ratio, standard cryogenic etching appears as a very stable, reproducible and clean process, then it can be used for MEMS devices, power microelectronics components [68] and TSV [69].

2.4. Defects currently observed in cryoetching

Classical etching defects, such as bowing and undercut, can be produced in cryoetching (figure 8). Their appearance mechanisms have been studied and they can be minimized or even cancelled. Dense black silicon can also be easily produced in cryoetching. This effect is discussed in section 5. Finally, as already mentioned, a CODE effect can occur at very low temperature.

2.4.1. Bowing. The mechanisms responsible for bowing formation in silicon cryoetching have been reported by Boufnichel *et al* [31, 32]. Once initiated, local bowing increases with process duration. Ions and radicals are both responsible for its generation. An increased self-bias favours its formation. The mask side slope can also contribute to the bowing development. Straight and vertical mask side slopes are preferred to prevent deflection of incident ions. The appearance of bowing can be controlled by adjusting the balance between ion flux and F/O relative density ratio [31]. More recently, it has been confirmed that the time dependence of lateral etching obtained in SF_6/O_2 plasma at ambient temperature was due to an increase in the scattering of ions reflected from the mask facets, which grows over time [70].

2.4.2. Undercut. Undercut is caused by spontaneous reactions of fluorine radicals. It develops at the very beginning of the etching process when bias stabilizes, as mentioned in [33]. Moreover, plasma ignition can induce a transient increase of the silicon surface temperature, which is not propitious for passivation layer implementation. When initiated, undercut

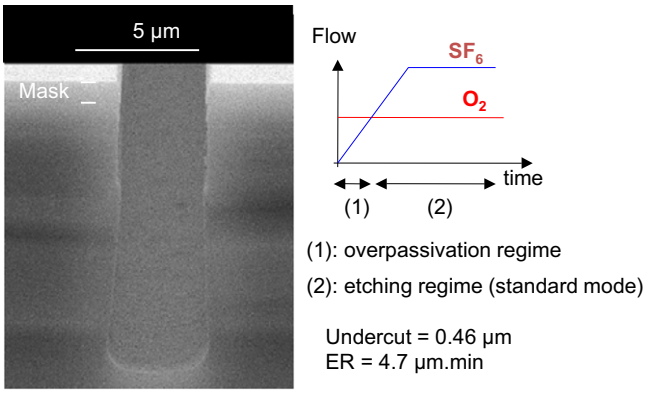

Figure 9. Anisotropic trench of 3.5 μm in aperture, 11 μm in depth, no bowing and no undercut, etched with an increase of the SF_6 flow during the first minute of the process. Reproduced with permission from [33]. Copyright 2005 Elsevier.

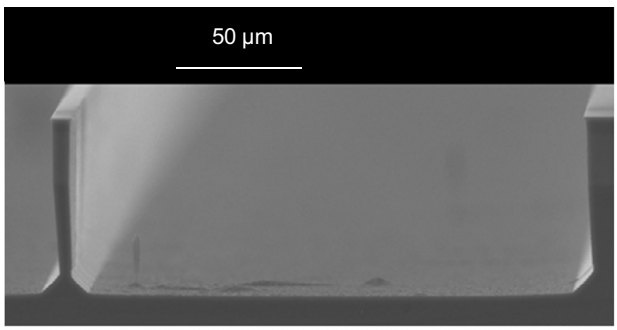

Figure 10. Evidence of the crystal orientation effect on 200 μm wide trenches etched by the cryogenic process (1000 W RF source, 35 V bias, 250 sccm SF_6, 27 sccm O_2, 3 Pa, −92 °C).

keeps growing linearly with process duration. A method has been suggested to get rid of this defect and to avoid its formation at the very beginning of the process, which consists in ramping SF_6 flow from 0 to the process nominal value within the first minute of the process (figure 9). In this case, the process starts in the over-passivating regime. When etching starts to dominate passivation, bias is stabilized and the SiO_xF_y layer is gently generated at the surface.

2.4.3. CODE. As reported by several groups [21, 27–30, 71], a CODE effect was evidenced at low substrate temperature. As observed in figure 10, (1 1 1) planes appear at the foot of a 200 μm wide trench etched at −92 °C. We can also notice that trench sidewalls have a negative slope. Gracium *et al* showed that this negative slope was a consequence of the CODE effect [71]. The etching component in the ⟨1 1 1⟩ direction induces the negative slope. As observed by Zijlstra *et al* [27], the etch rate of Si(1 0 0) is larger than that of Si(1 1 1). They report that Si(1 0 0)/Si(1 1 1) etch rate ratio increases when decreasing the temperature. A maximum is reached at around −80 °C.

The CODE can significantly modify the pattern geometry. In figures 11(*a*) and (*b*), it is shown that an initial circular hole pattern turned to a square shape due to this effect. In thermal oxidation, it is well known that the oxidation process is faster on Si(1 1 1) wafers [72]. This is due to the difference of surface density of silicon atoms. Moreover, on (1 1 1) planes, a single

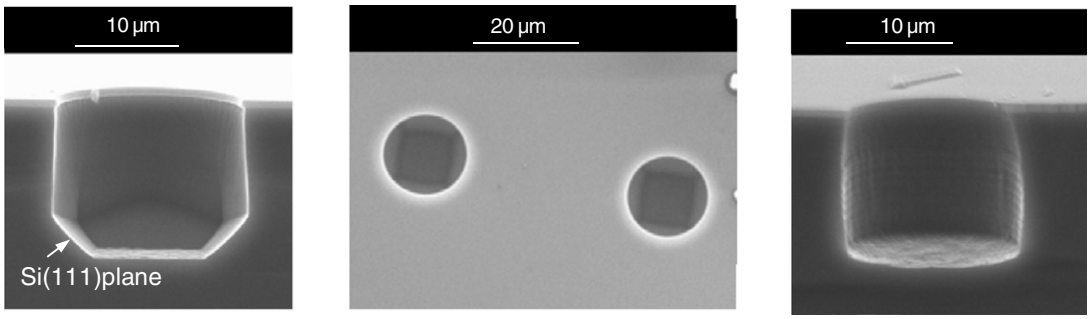

Figure 11. Side (*a*) and top (*b*) views of the crystallographic effect on hole patterns. (*c*) Profile obtained using the cycled amorphization process.

dangling bond is available from the silicon atoms of the surface. It seems that this configuration favours passivation. In thermal oxide processes, it is well known that crystal planes that have higher densities of atoms oxidize faster. In silicon cryoetching, (1 1 1) planes seem to be more efficiently passivated than (1 0 0) planes, which could be the reason why the etch rate is lower in ⟨1 1 1⟩ directions.

As mentioned in reference [71], it is possible to avoid this effect by raising the process temperature a little. However, in some cases, raising the temperature will induce slopes that are too positive in other smaller patterns of the mask.

Another method was recently suggested by Mekkakia-Maaza *et al* [73], which consists of alternating amorphization steps by Ar/O_2 plasma and etching steps by SF_6/O_2 plasma at low temperature. The role of the argon ion bombardment is to amorphize the surface before each cryoetching step. The crystallographic was suppressed using this method (see figure 11(*c*)).

3. Passivation mechanisms in silicon cryoetching

As already mentioned, the fine control of the passivation layer formation is a key issue in the cryoetching process. A passivation that is too strong would lead to the appearance of black silicon whereas a too weak passivation would initiate irreversible defects.

The profiles of a 5 μm wide trench pattern are shown in figure 12. They were obtained after etching processes at different substrate temperatures, with or without oxygen, and with or without ion bombardment. The other parameters (such as source RF power, process duration and pressure) were kept constant.

Without ion bombardment, when SF_6 is the only injected gas, an isotropic profile is obtained whether the temperature is between +30 °C and −110 °C. At −110 °C, we can hardly see a very slight modification of the profile. This is in perfect agreement with the results reported by Bartha *et al* [11]. When O_2 is added to SF_6, the profile is still isotropic and similar to those obtained without O_2. But at −80 °C, a significant modification is observed: some faceting appears and the profile is no longer isotropic. At −110 °C, in the same conditions, the profile shows an accentuated faceting effect. Lateral etching is not stopped and the profile has a lozenge shape. When ion bombardment is added, the profile is modified, even at +30 °C, especially at the bottom of the profile. The effect is accentuated at −50 °C. A trench forms at −80 °C but with a positive slope, and large bowing and undercut. Finally, at −110 °C, a nice trench shape is produced with a slightly negative slope and a remaining crystallographic effect at the foot of the trench. In these final conditions, it is clear that an efficient passivation layer was formed. Consequently, low temperatures, oxygen flow, and ion bombardment are required to build an efficient passivation layer in silicon cryoetching.

The next section will inquire into the composition and properties of this passivation layer. It will also examine the role of each process gas. In addition, it will determine how the passivation efficiency may be enhanced. Many different characterization experiments have been carried out in order to better understand the passivation mechanism at a cryogenic temperature, which are summarized here.

3.1. Ex situ XPS experiments

Ex situ XPS analysis was first carried out to analyse the passivation layer composition [43]. Etched samples were cleaved along a 10 μm wide trench and analysis was performed on a 20 μm diameter area at different locations on etched sidewalls (figure 13), and on cleaved but not etched parts (point C in figure 13). Many precautions were taken to perform these experiments, especially to avoid oxidation by the ambient air during the cleavage of the sample and its transportation to the XPS equipment. In order to prevent natural oxidation, all manipulations and transportations were carried out in a pure nitrogen atmosphere. Cleavage was performed in a glove box where the oxygen content was measured and controlled.

An example of XPS spectrum is given in figure 14. The analysis was performed on the A zone; that is, near the top of the trench. Only a very weak intensity of the Si–O peak, much weaker than that obtained when native oxide is analysed, can be observed.

Details of the analysis are given in [43]. A series of experiments and SEM observations were carried out to check that a passivation layer as thin as native oxide could not protect efficiently vertical sidewalls from lateral etching. The conclusions of this study are clear: the passivation layer is removed when the wafer is brought back to atmospheric pressure, and cryogenic etching provides a very clean surface of the etched structure after etching. We also showed that it was possible to rebuild the passivation layer when removed,

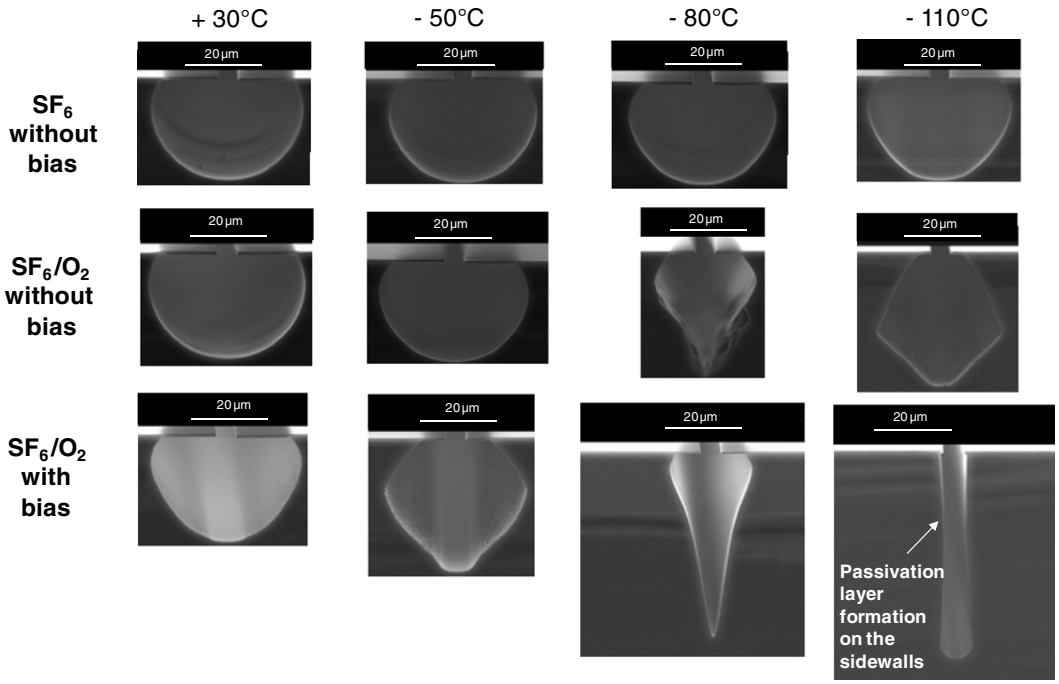

Figure 12. Profiles of a trench pattern obtained for different substrate temperatures, with or without oxygen, and with or without ion bombardment. Other parameters (such as pressure, RF power, process duration) are kept constant. Reproduced with permission from [44]. Copyright 2005 American Institute of Physics.

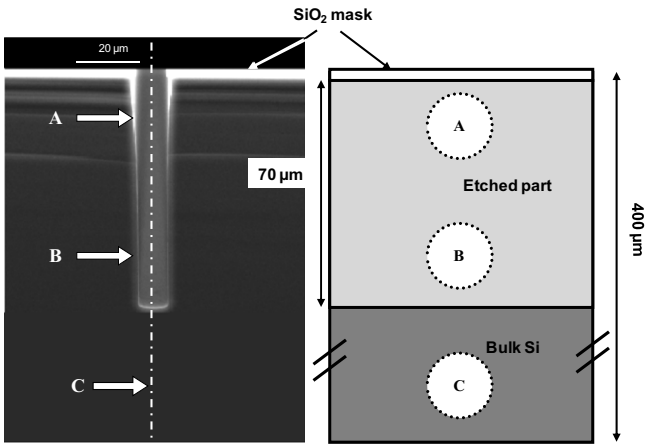

Figure 13. Left: SEM picture of the analysed trench after etching (right) scheme representing the front view of the sidewall and the different analysed zones [43].

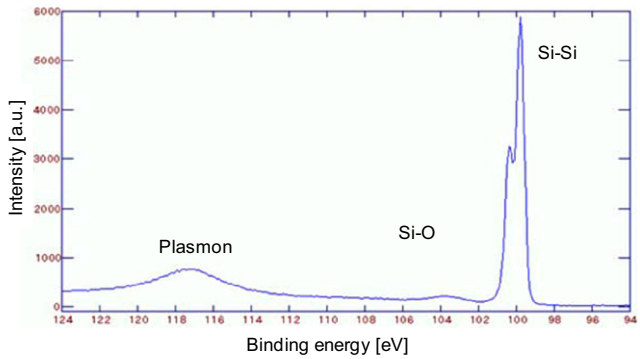

Figure 14. Region of interest of an XPS spectrum showing the Si-2p part [43].

but an intermediate process step had to be inserted before the standard etching conditions [43].

3.2. Desorbed species analysed by mass spectrometry

Since the passivation layer seems to desorb after the etching process, *in situ* analysis had to be performed. To this aim, a mass spectrometer was installed on the reactor to analyse the plasma during the process and the desorbed species during the wafer warm-up. The principle of the experiment is schematized in figure 15.

First, a standard SF_6/O_2 cryoetching process was run to etch the 50, 20, 10, 8 and 6 μm wide trenches, which are shown on the SEM picture (figure 15). The wafer temperature was $-110\,^{\circ}C$, SF_6 and O_2 flows were 20 sccm and 5 sccm respectively. The source power was 800 W and bias power was set to 110 W. The etch process duration was 20 min. Again, both ARDE and CODE effects appear clearly on the SEM picture. These anisotropic etched structures show that an efficient passivation layer was created in these process conditions. Afterwards, residual gas was first evacuated. Then, the throttle valve was closed to analyse the desorbed species during the wafer warming. Spectra between 80 and 90 amu were acquired in residual gas analysis (RGA) mode at four different temperatures (figure 16). This *m/e* range is interesting for this experiment because different species (such as SiF_x, SF_x and SOF_x) can be monitored.

At $-110\,^{\circ}C$, just after the plasma process, SO_2F^+, SOF_2^+ and SOF_3^+ lines are present. As the wafer is heated to $-70\,^{\circ}C$, a significant increase of SO_2F^+ and SOF_2^+ peaks is observed

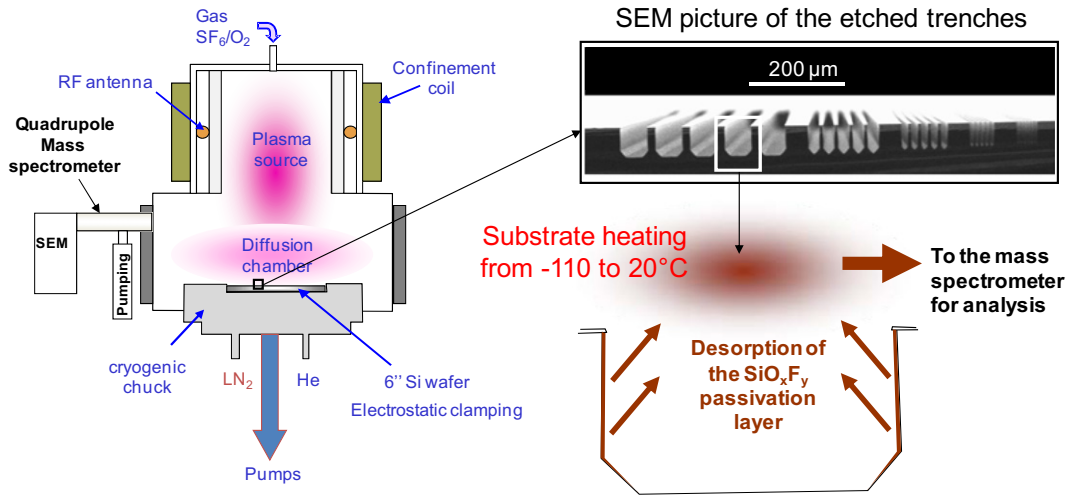

Figure 15. Scheme of principle of the mass spectrometry analysis experiments.

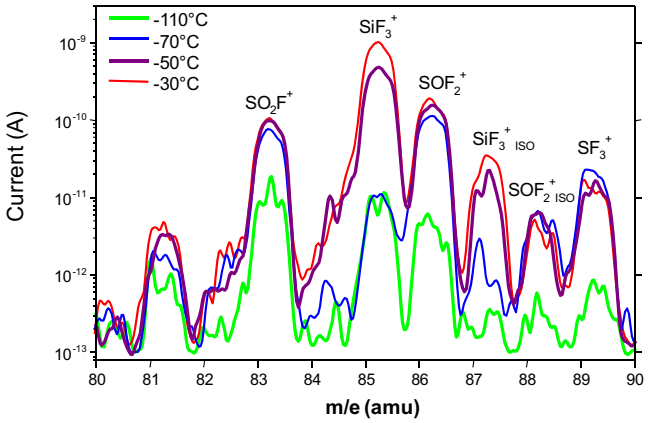

Figure 16. Mass spectrometry spectra at four substrate temperatures −110, −70, −50 and −30 °C after a standard cryoetching process. Reproduced with permission from [44]. Copyright 2005 American Institute of Physics.

whereas the SiF_3^+ line intensity remains constant. The SF_3^+ line also appears at this temperature. The spectrum at −50 °C shows a large increase of the SF_3^+ peak whereas other peak intensities remain more or less constant. Finally, between −50 and −30 °C, the SiF_3^+ line keeps increasing and other lines do not vary significantly. SiF_3^+ is the main line of the fragmentation spectrum of SiF_4. It seems that SiF_4 desorption occurs beyond −70 °C. This result may appear surprising since the boiling point of SiF_4 is at a much lower temperature, especially at low pressure. SO_2F^+ and SOF_2^+ mainly come from the dissociation and ionization of the SO_2F_2 molecule.

A more detailed description of the experiment can be found in [44]. In particular, many other species were analysed using the multiple ion detection (MID) mode to get more resolved data acquisition in terms of desorption temperature. Note that no SiO_xF_y species were detected by mass spectrometry in this experiment. Analysis was also performed in over-passivating regimes and after SiF_4/O_2 plasma at low temperature. Each time, the same trend was obtained: SO_xF_y and SF_x species main desorption occurred between −110 and −80 °C and SiF_4 main desorption between −80 and −40 °C. This experiment confirmed the fact that the passivation layer was desorbing during the wafer warm-up. But, at this point, the desorption mechanism is not yet clear.

3.3. Passivation layer formation tests

From mass spectrometry analysis, it was found that SiF_4 was desorbing during the wafer warming. One can wonder if this molecule plays an important role in the passivation mechanism. In particular, would it be possible to create a passivation layer using SiF_4 gas? To answer this question, the following test experiment was performed. An isotropic cavity was etched without bias and without oxygen. The profile is shown in figure 17. This process is called INI. The obtained profile is very reproducible and serves as a reference for the other experiments. If we add 3 min of the same process, but with 37 V bias (FIN process), the profile shown in figure 17 is obtained. It has basically the same isotropic shape as the reference profile, but the cavity is larger. But, if a 1 min long SiF_4/O_2 plasma step is inserted between INI and FIN steps, two cavities are created. By comparing the different obtained profiles, one can see that the upper cavity fits perfectly with the reference profile. So we can conclude that the SiF_4/O_2 plasma deposited a passivation layer, which protected the first cavity. Due to ion bombardment induced by the FIN step, this passivation layer was removed at the bottom and a second cavity was formed without over-etching the first cavity. So, this experiment shows that SiF_4/O_2 plasma can generate an efficient passivation layer.

To understand more precisely what mechanism is involved in this passivation step, other tests were carried out. To first check if the mechanism was relying on a SiF_4 or SiF_x physisorption, the inserted step was replaced by a flow of SiF_4 or by a plasma of SiF_4 without oxygen. In both cases, a large isotropic cavity formed, perfectly fitting with the one obtained after the 3 min FIN process, without an inserted step [44], which showed that SiF_4 or SiF_x physisorption was not the mechanism responsible for the passivation layer formation. It also confirmed that O_2 was necessary to make an efficient passivation layer.

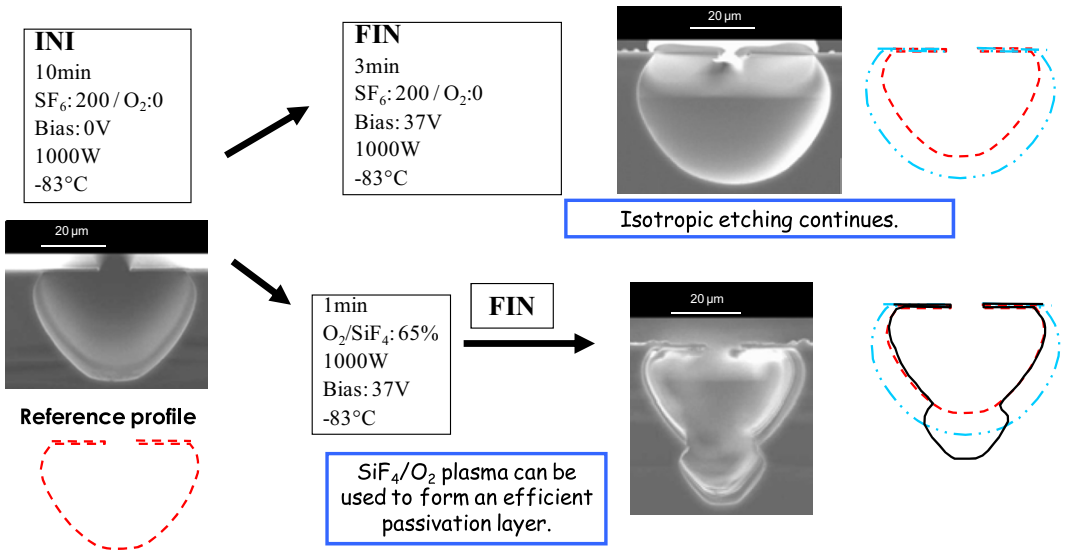

Figure 17. Passivation layer formation test with SiF_4/O_2 plasma. Profile contours are represented at the side of the SEM pictures for comparison. Reproduced with permission from [44]. Copyright 2005 American Institute of Physics.

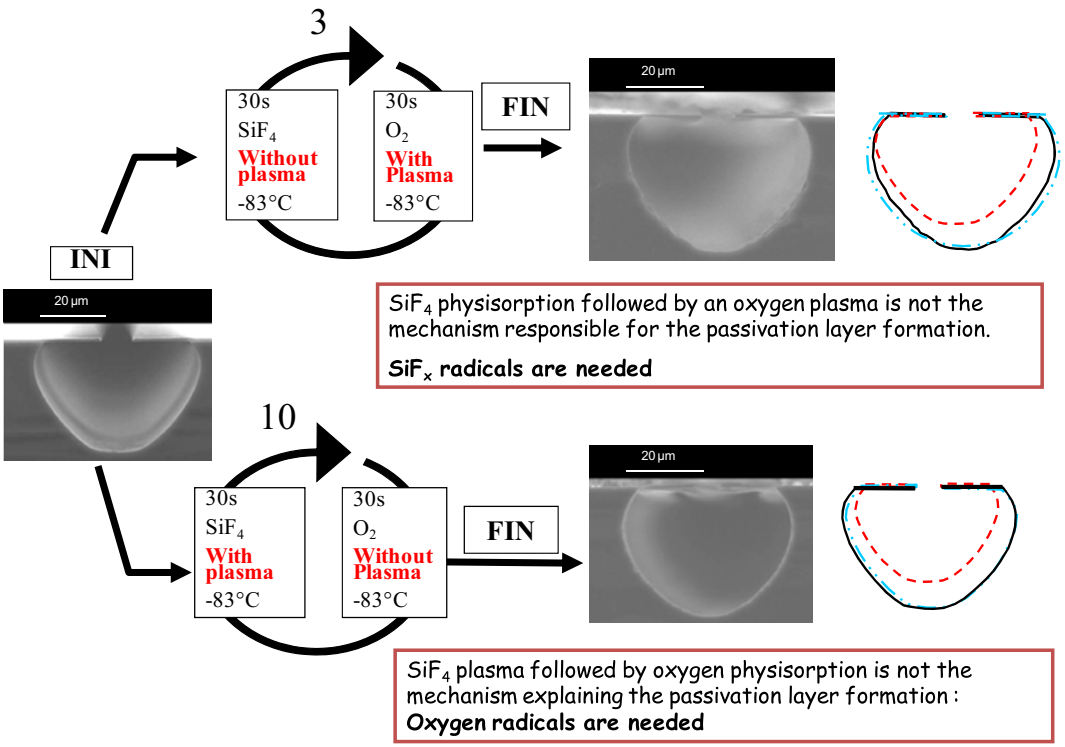

Figure 18. Etched profiles obtained after a 10 min standard isotropic etching process (INI) followed by passivation construction steps and finished by the 3 min FIN etched process. Passivation construction steps consist of three alternations of SiF_4 flow without plasma and O_2 plasma in the first case and ten alternations of O_2 flow with SiF_4 plasma in the second case. Profile contours are represented for comparison: the dashed line contour is the INI profile, the dotted–dotted–dashed line contour represents the FIN profile, and the solid line is the contour of the etched structure profile. Reproduced with permission from [44]. Copyright 2005 American Institute of Physics.

Other tests were carried out by separating O_2 and SiF_4 in two distinct steps. In the first experiment, which is shown in figure 18, SiF_4 flow without plasma and O_2 plasma were alternated three times to see if SiF_4 molecules were first physisorbed and then oxidized. But, obviously no efficient passivation layer was created by this method. It seems that SiF_x ($x \leqslant 3$) radicals are necessary. Then, in the second experiment, which is shown in figure 18, SiF_4 plasmas with O_2 flow without plasma were alternated ten times. Again, this step was not efficient to create the SiO_xF_y layer. This means that O radicals and SiF_x radicals are both necessary to build an efficient passivation layer.

Finally, O_2 plasmas and SiF_4 plasmas were separated and alternated. Figure 19 gives the results as a function of the cycle number. If we alternate only once a 30 s pure SiF_4 plasma with a 30 s pure O_2 plasma, it is not sufficient to create an

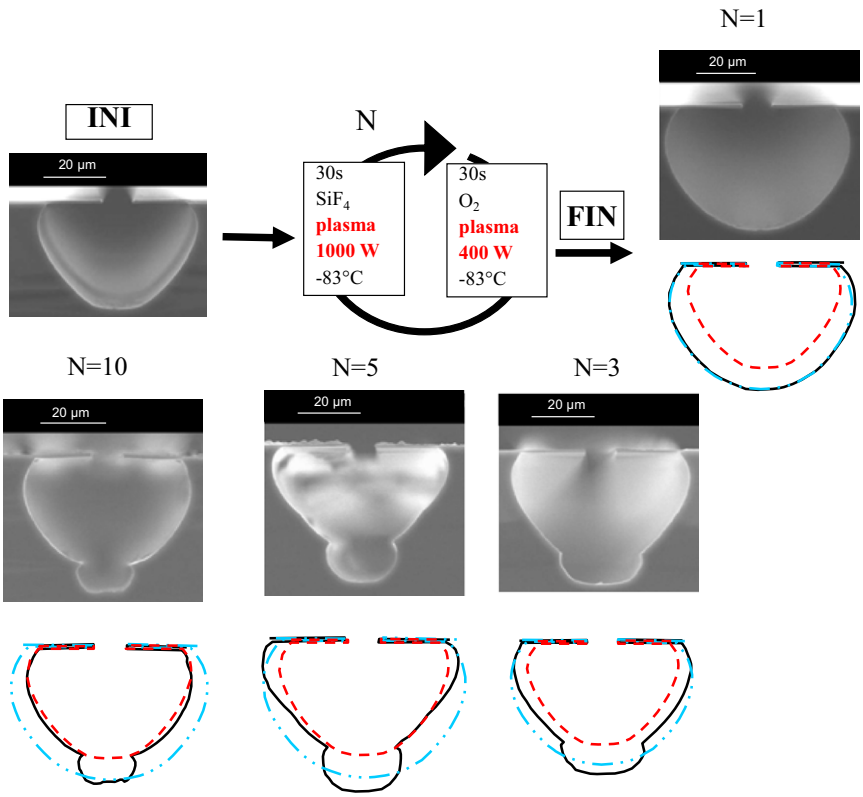

Figure 19. Etched profiles obtained after a 10 min standard isotropic etching process (INI) followed by passivation construction steps and finished by the 3 min FIN etched process. Passivation construction steps consist of alternations of SiF_4 and O_2 plasmas. N is the cycle number. Profile contours are represented for comparison: the dashed line contour is the INI profile, the dotted–dotted–dashed line contour represents the FIN profile, and the solid line is the contour of the etched structure profile. Reproduced with permission from [44]. Copyright 2005 American Institute of Physics.

efficient passivation layer. For three alternations, a second cavity forms, but the passivation layer seems too thin and too weak to withstand the 3 min FIN etching process and the first cavity is a little over-etched. After five alternations, the obtained cavity fits better to the reference profile, but there is still some over-etching at the top of the cavity. Finally, after ten alternations, the first cavity fits perfectly to the reference profile, which means that an efficient passivation layer was deposited during the alternations of SiF_4 and O_2 plasmas. This experiment shows that O atoms react with SiF_x radicals at the surface to form the SiO_xF_y layer.

From these experiments, one can conclude that SiF_4 etch by-products can participate to the passivation layer formation, and even reinforce it. However, it is known that it is possible to run anisotropic cryoetching on isolated and small features from which SiF_4 production is low and does not participate to passivation. In this case, SiF_x sites are created at the surface during the etching and are oxidized by oxygen radicals, but the passivation layer is probably thinner and more fragile than in the case where a large amount of SiF_4 is produced.

3.4. In situ ellipsometry analysis of the passivation layer formed by SiF_4/O_2 plasma

In situ ellipsometry analysis was carried out on silicon wafers cooled at low temperature and exposed to SiF_4/O_2 plasma. A system of biased grids was placed above the wafer to reduce ion bombardment and protect the fragile deposited layer. This way, ion density was reduced by two orders of magnitude. More details are given in [46].

The film thickness evolution is shown in figure 20.

When the plasma is on, the film grows linearly with a deposition rate of 6 nm min^{-1} during 15 min. Then, the plasma is switched off and the wafer is warmed slowly while ellipsometric spectra are acquired. As observed on the graph, the film thickness is quite constant from −100 to −80 °C, then it slightly decreases from −80 to −60 °C. Finally, a significant decrease is observed from −60 to +20 °C. The remaining layer is 18 nm thick, which means that more than 80% of the film desorbed. These results are in good agreement with mass spectrometry analysis. To complete this set of experiments of characterization and to understand the desorption mechanism, *in situ* XPS analysis was performed, and is presented in the next section.

3.5. In situ XPS experiments

A dedicated small ICP reactor was mounted and installed on an XPS chamber at IMN at Nantes (figure 21). The silicon sample was installed on a cryogenic substrate holder, itself mounted on a rod that could be translated from the plasma reactor to the XPS chamber while keeping the sample at a cryogenic temperature. Before plasma treatment, the sample was submitted to a 4 min long SF_6 plasma to clear the native

oxide layer and clean the silicon surface. Then, the sample was cooled down to a low temperature. The experiments were carried out under SF_6/O_2 plasma in an over-passivating regime (20 sccm of SF_6 and 13 sccm of O_2). Although the sample and the substrate holder could be independently biased using a dedicated power supply, they were left at the floating potential to limit ion bombardment and grow a SiO_xF_y layer on a flat surface. More details on the experiment can be found in [48].

After a 30 s long plasma, the sample was transferred to the XPS chamber for analysis. XPS spectra were taken every 25 or 30 °C. Spectra in the range 800–500 eV and 400–0 eV binding energy are shown in figure 22. The peaks at 150 eV and 100 eV are attributed to Si 2s and Si 2p respectively. No sulfur line was observed: sulfur could be removed by SOF_4 and SO_2F_2 formation at the surface as reported in [45]. A non-negligible amount of carbon (C 1s) was also detected: they probably come from residual gases from remaining present in the chamber. It is well known that very reactive fluorine species can react with hydrocarbon compounds, which are adsorbed on the inner walls of the ICP reactor. The line evolution can be examined carefully versus temperature. While Si peaks can be hardly observed at low temperatures, their intensity increases by heating the surface. In parallel, the lines attributed to carbon decrease.

These results are summarized in figure 23, where the percentage of each element detected at the surface is given through a bargraph. Fluorin concentration tends to decrease below −50 °C. Oxygen concentration remains more or less constant and silicon concentration at the surface tends to increase.

Si 2p spectrum evolution for four different temperatures is shown in figure 24. It is quite interesting to notice the evolution of the peaks coming from SiO and SiF bonds and of the Si–Si bonds (Si2p 1/2 and Si2p 3/2 peaks): the ratio of the two peaks is inverted during the sample warm-up. This clearly shows the evolution of the surface, which is first rich in SiO and SiF bonds and then, during the sample warm-up, becomes rich in Si–Si bonds. This analysis confirms the modification of the surface during the sample warm-up and is consistent with other results reported in the previous sections. A global interpretation of the passivation mechanism and the layer desorption is suggested in the next section.

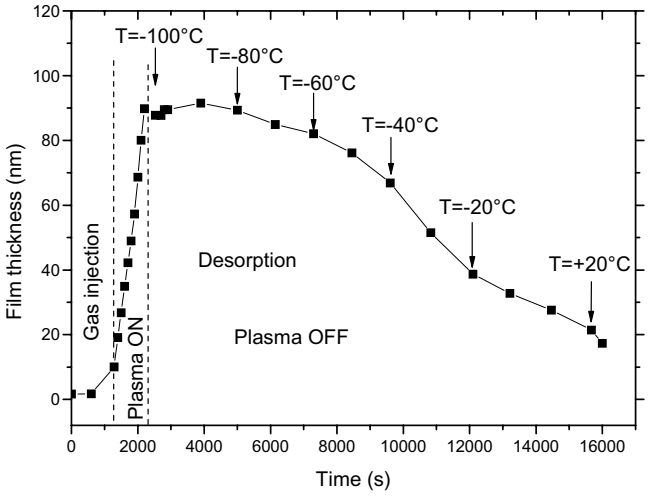

Figure 20. Evolution of the SiO_xF_y film thickness under a SiF_4/O_2 plasma at −100 °C (plasma ON) and during the wafer warm-up (plasma OFF). Reproduced with permission from [46]. Copyright 2007 Elsevier.

3.6. Interpretation and conclusion on the passivation layer formation and desorption

From previous sections, several properties of the passivation layer in silicon cryoetching were highlighted. We have first shown that oxygen, low temperature, and a quite low ion bombardment are necessary to create an efficient passivation layer to etch trenches anisotropically using the cryoetching process. Then, *ex situ* XPS analysis showed that passivation layer was not stable and was desorbed when the sample was heated to ambient temperature. By analysing the desorbed species by mass spectrometry, we found out that desorbed species were mainly composed of SiF_4 molecules and that the main desorption was occurring from −70 to 30 °C. Most of the passivation layer is self-removed, as observed by *in situ* ellipsometry. Moreover, it was shown that it is possible to create a robust passivation layer with SiF_4 and O_2 plasma at low temperature. Finally, *in situ* XPS analysis revealed that the chemical composition of the surface was changing

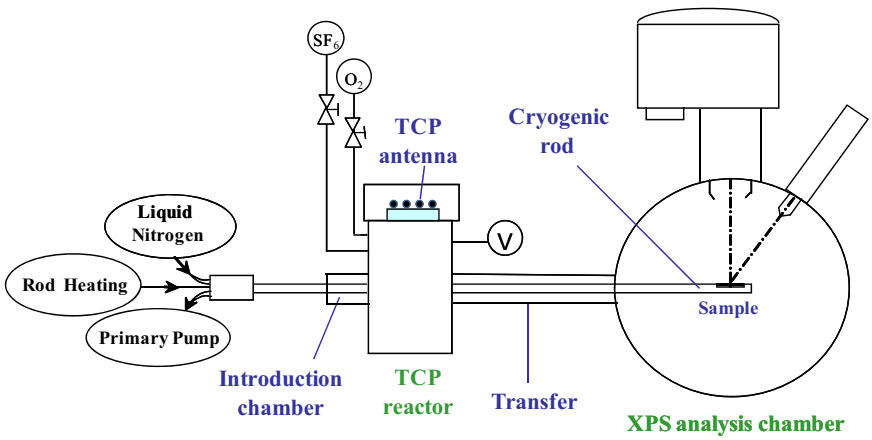

Figure 21. Diagram of the *in situ* XPS analysis.

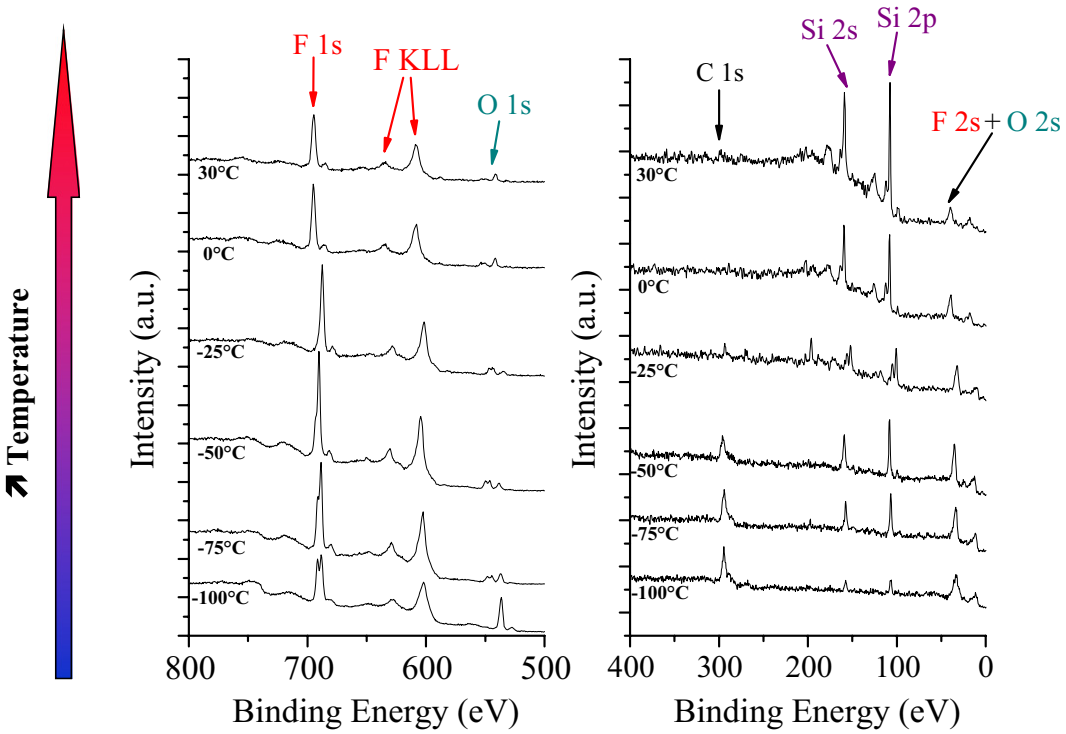

Figure 22. XPS spectra evolution during the sample warm-up after a 30 s SF_6/O_2 plasma in an over-passivating regime. Reproduced with permission from [48]. Copyright 2009 American Institute of Physics.

during the sample warm-up. We can now suggest a mechanism of adsorption and desorption of the passivation layer in the cryoetching of silicon.

The passivation layer formation tests showed that SiF_x radical from SiF_4 dissociation adsorb at the surface and react with O atoms to form the SiO_xF_y passivation layer. Zhang and Fischer had already reported that the major contribution to SiOF film deposition was made by SiF_x species [74]. If SiF_x radical concentration is low (low etch rate or small etched surface area), then cryoetching can still work, but in this case the mechanism is a little bit modified: fluorine radical diffuse within few monolayers to form SiF_x at the very surface of the etched area, oxygen radicals from the plasma then react with these sites to form SiO_xF_y layers, which are stable at low temperature. Once formed, we can assume that the surface is rich in fluorine and that the stoichiometry is probably closed to $SiOF_3$. Then, by increasing the surface temperature, the surface is reorganized. Fluorine atoms diffuse at the surface and replace oxygen sites to form volatile SiF_4 molecules, which desorb from the surface. This phenomenon would occur between −70 and 30 °C. This interpretation can explain why SiF_4 desorbs in this range of temperatures whereas SiF_4 is also volatile at lower temperatures. The mechanism is illustrated in figure 25.

Some other experiments are reported in SiF_4/O_2 plasmas at room temperature, especially for low-k material studies [75]. But, in this case, the oxygen concentration is much higher [74, 76]. In particular, it is shown in [77] that when the fluorine atoms are incorporated into the SiO_2 film, the Si–O–Si bond network is broken. Consequently, fluorine incorporation makes the bond structure more open and lowers the density of the film. This mechanism might be reduced at low temperature.

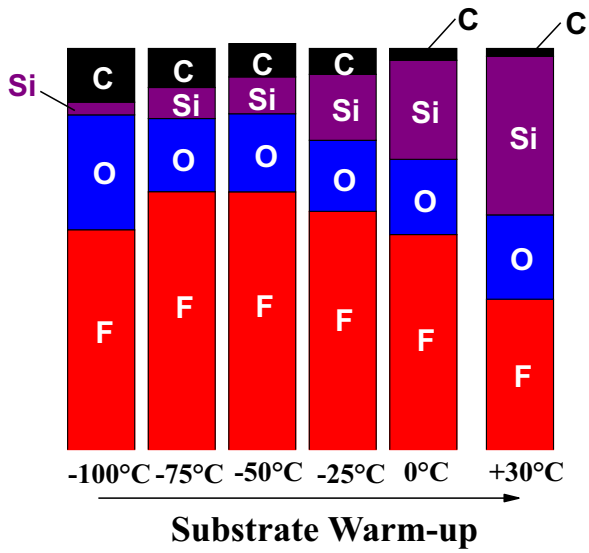

Figure 23. XPS atomic quantification during the substrate warm-up. Reproduced with permission from [48]. Copyright 2009 American Institute of Physics.

4. Cyclic cryogenic etching

4.1. O_2 alternations

In order to reduce undercut, Boufnichel *et al* have suggested to pulse the oxygen flow during the cryoetching process. The result is shown in figure 26. As observed on the SEM picture, some oscillations appear at the sidewall due to the pulse mode [33]. Oxygen pulses favours passivation, which induces positive slopes. Then, when oxygen is reduced, a more

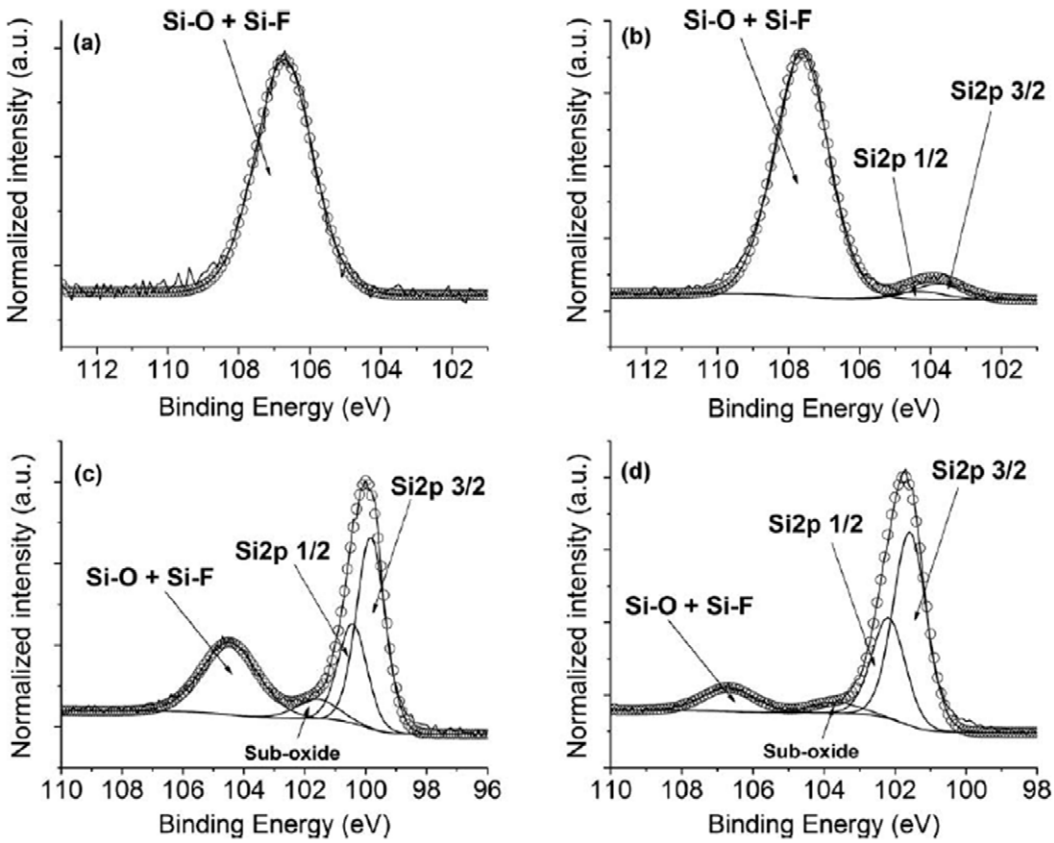

Figure 24. Evolution of Si 2p peak shape during the sample warm-up. (*a*) $T = -100\,^{\circ}$C, (*b*) $T = -50\,^{\circ}$C, (*c*) $-25\,^{\circ}$C and (*d*) $30\,^{\circ}$C. Reproduced with permission from [48]. Copyright 2009 American Institute of Physics.

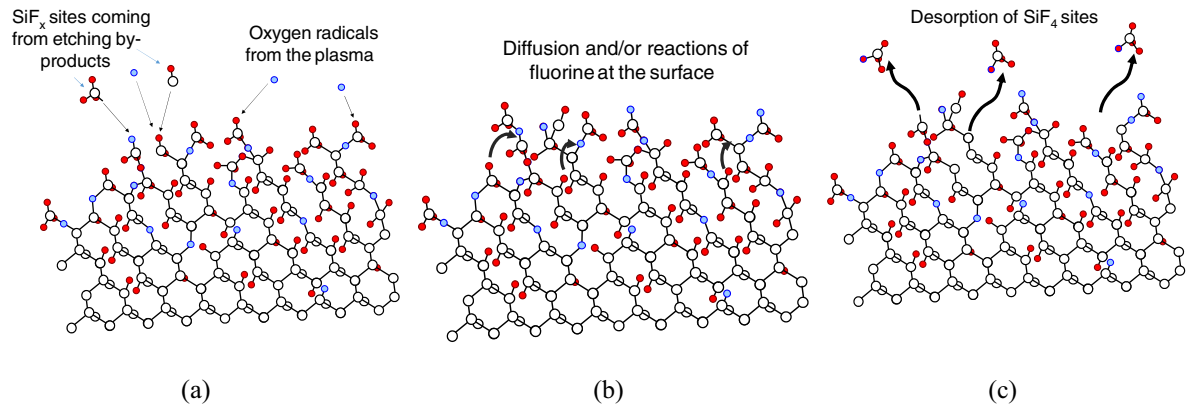

Figure 25. Illustration of passivation and desorption mechanisms involved in Silicon cryoetching: (*a*) SiF_x and O radicals deposit at the surface during the plasma process; (*b*) After plasma, during the wafer warm-up, the surface is reorganized and SiF_4 molecules are formed by fluorine diffusion and chemical reactions; and, (*c*) when formed, SiF_4 molecules desorb from the surface.

negative slope is obtained. Consequently, a periodicity on the trench sidewall is clearly observed.

This cyclic SF_6/O_2 cryoetching technique was successfully tested by another group a few years later [53]. The authors provided several recipes where the O_2 flow and/or process pressure were varied at each cycle. An example of their results is given in figure 27. They also compared this method with the Bosch process in terms of etch rate, selectivity and uniformity variation.

This method has several advantages: it exhibits vertical sidewalls, minimizes Si grass formation and is relatively independent of mask geometry for microscale features. Oxygen pulsed plasmas were also studied and compared with standard cryoetching process and Bosch process [78]. However, the passivation layer remains quite fragile in this process. In the next section, the so-called STiGer process is presented and provides a more robust passivation layer.

4.2. The STiGer process

As reported in previous sections, SiF_4 can play an important role in the passivation layer formation. In order to reinforce

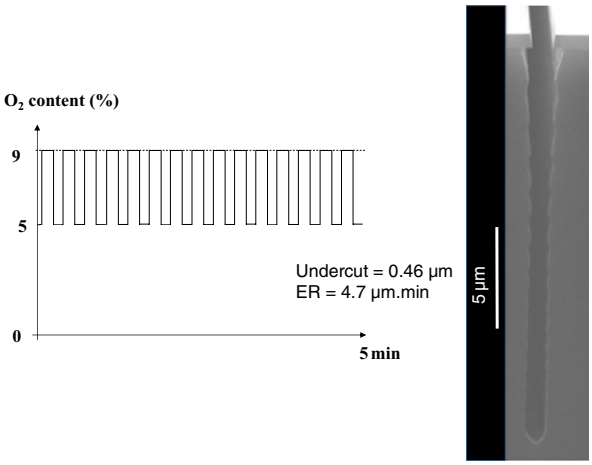

Figure 26. Oxygen pulsed process introduced by Boufnichel *et al* in order to reduce undercut. (right) SEM picture of the obtained profile after a 5 min process. Reproduced with permission from [33]. Copyright 2005 Elsevier.

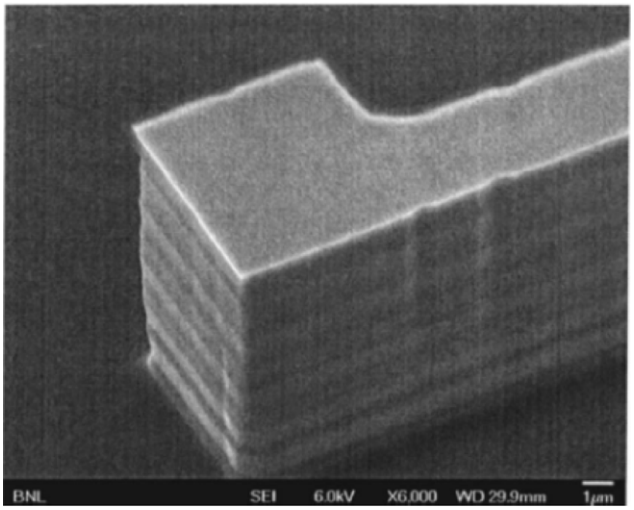

Figure 27. Dark and bright layer-like features visible in this etch are indicative of the cyclic phases utilizing varied oxygen content. The apparent thicknesses of the layers are proportional to the etching periods. Reproduced with permission from [53]. Copyright 2008 American Institute of Physics.

the passivation layer, some tests were carried out by alternating SiF_4/O_2 plasma passivation steps with SF_6 plasma etching steps. The first test was carried out using quite long steps: 1 min long SF_6 plasma etching plasmas were alternated five times with 30 s long SiF_4/O_2 plasmas at −83 °C. The result is shown in figure 28(*a*). Isotropic cavities are formed and superimposed. Note that the first is bigger than the others, because the subsequent etch steps are all preceded by a depositions step. The same experiment was reproduced, but at 0 °C. The result is also shown in figure 28(*b*). For comparison, the first cavity obtained at −83 °C is shown in white line on the figure. A single large cavity is obtained at 0 °C, which proves that the passivation layer is effective only at low temperature.

By reducing the duration of each cycle, high-aspect-ratio structures can be obtained, such as the trenches shown in figure 29. In this particular example, 0.8 μm wide trenches were etched with etch cycles of 4 s and deposition steps of 2 s. This process was patented in 2008 [52]. One can clearly observe the scalloping effect, just like in the Bosch process. The etch rate is comparable to that achieved using the Bosch process.

It is also possible to alternate long standard anisotropic etching with SF_6/O_2 with short deposition steps, as reported in [51]. In this case, the deposition step is used to reinforce the sidewall passivation. It can also help in adjusting the sidewall slope and tuning it from negative to vertical.

The STiGer process is quite close to the Bosch process in its principle. One can wonder then about why it may be useful to use it instead of the Bosch process. The fact that liquid nitrogen has to be used to cool down the substrate can clearly appear as a drawback for its implementation in clean room facilities for industrial production. However, several advantages exist when using this process. First, although the etch rate is not greater than that obtained with the Bosch process, the number of etched wafers per hour can be higher using the STiGer process due to the fact that no cleaning steps are necessary in the STiGer process. Since SiO_xF_y deposition occurs only on very cold surfaces, there is no deposition on the reactor walls and so, no process drift was observed. Moreover, since the passivation layer is self-removed when the wafer is warmed back to ambient temperature, the etched surfaces are clean and it is not necessary to insert a cleaning step to remove the passivation layer.

STiGer process can also be advantageous compared to the standard cryoetching process. In figure 30, we show the trench bottom width of 10 μm wide trenches after a 10 min process using standard cryoetching and STiGer processes. In the STiGer process, the slopes are the same over a wide range of temperatures (from −92 to −72 °C). In standard cryoetching, the profile is very dependent on temperature: the bottom width varies from 9 to 2 μm in this example in a 10 °C range of temperature.

The STiGer process was used to etch very high-aspect-ratio trenches for capacitor integration in 3 dimensions. An example is given in figure 31, where 0.8 μm wide and 38 μm deep trenches are shown (aspect ratio of 47). However, if one zooms to the trench top, a new defect that we have named 'extended scalloping' can clearly be observed, which corresponds to the pits that start from the scalloping defects and propagate obliquely. This defect is unwanted, especially for deposition steps subsequent to deep etching. This extended scalloping has been studied by Tillocher *et al* [79]. It was found that ions are mainly responsible for the appearance of this defect. The mask slope was not vertical enough and was favouring specular reflection of ions in this area. This effect could be reduced by oxygen addition in the etch cycle in the first minutes of the process.

Note that scalloping can also be removed after the process by using low concentrated alkaline solutions at low temperature [80].

Although the STiGer process gives some very promising results and performances, the temperature has to be maintained below −70 °C, which requires liquid nitrogen. In the next section, another process that does not require such a low temperature is described.

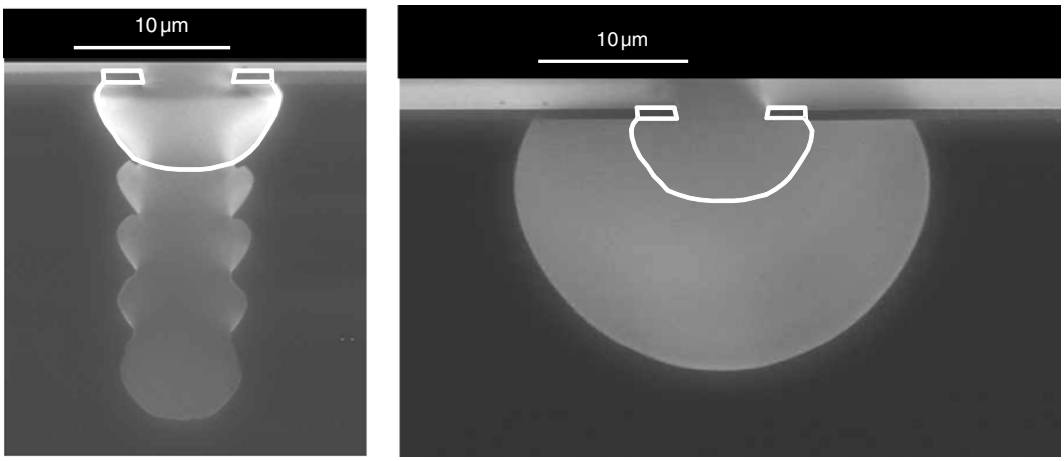

Figure 28. Profile of a 4 μm wide trench obtained after four alternations of etching (1 min SF_6 plasma) and passivation (30 s SiF_4/O_2 plasma) plus one last etch step (SF_6 plasma) at −83 °C (*a*) and at 0 °C (*b*). Reproduced with permission from [91]. Copyright 2008 The Electrochemical Society.

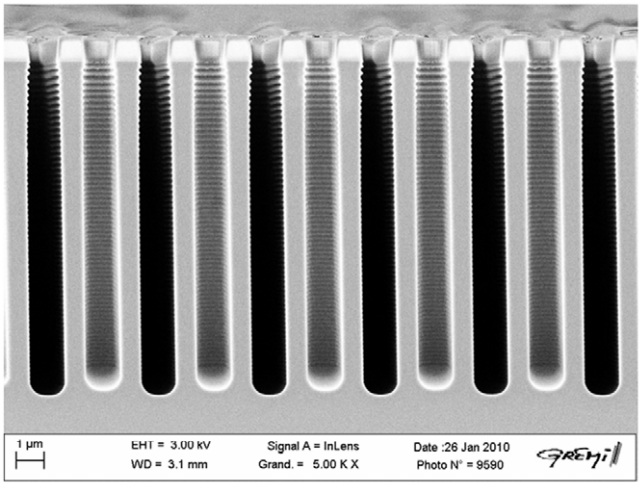

Figure 29. 0.8 μm wide and 12 μm deep trenches etched with the STiGer process during 5 min.

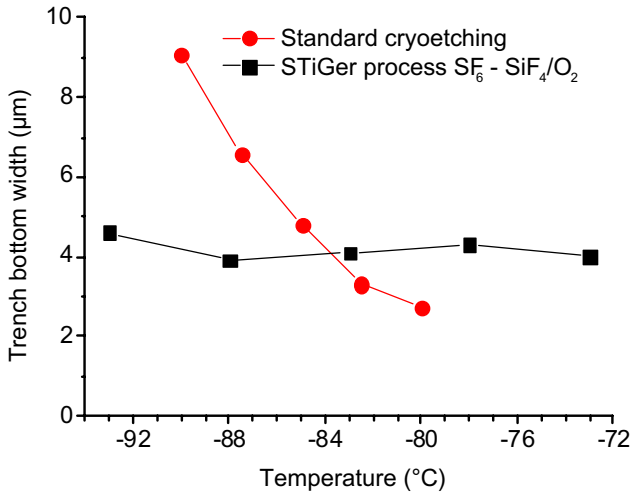

Figure 30. Comparison of the trench bottom width of 10 μm wide trenches obtained after 10 min process using standard cryoetching (red circles) and STiGer (black squares) processes. Reproduced with permission from [91]. Copyright 2008 The Electrochemical Society.

4.3. Tests with chlorine based chemistries

Chlorine based chemistries have been investigated in order to develop new silicon deep etching processes working at substrate temperatures higher than −30 °C without using fluorocarbon passivating gases. Gas mixtures containing $SiCl_4$ and SF_6 were first tested in a continuous plasma. The idea was to deposit $SiCl_x$ species at the vertical sidewalls to prevent etching by fluorine radicals. These experiments are described in detail in [81]. The temperature was set to 0 °C. It was shown that a $SiCl_x$ layer was also deposited on the chamber walls. A reaction scheme is proposed in [81] to explain how its desorption was assisted by fluorine and sulfur radicals. This mixture did not provide good enough results in terms of etch profiles. Another process based on alternated steps of SF_6 plasmas and $SiCl_4/O_2$ plasmas was proposed at −20 °C, the results are reported in [82]. The role of $SiCl_4/O_2$ plasmas was to form an efficient SiO_xCl_y passivation layer at

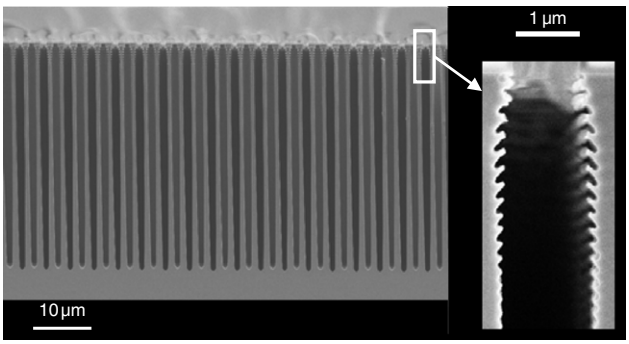

Figure 31. High-aspect-ratio (47) trench structures obtained with the STiGer process and (inset) emphasis on the 'extended scalloping' defect.

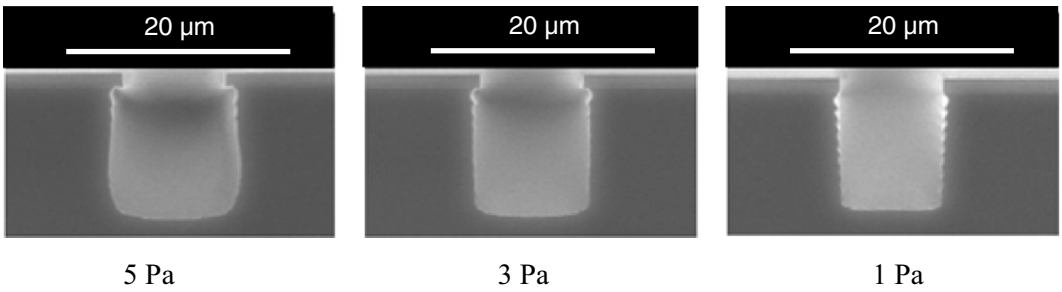

Figure 32. Influence of the $SiCl_4/O_2$ plasma pressure on 10 μm wide trenches. Profiles were obtained after 10 alternations of SF_6 plasma etch steps (100 sccm, 5 Pa, 1000 W, −50 V, 30 s, −20 °C) with $SiCl_4/O_2$ passivation steps ($SiCl_4$ 50 sccm, O_2 25 sccm, 1000 W, −30 V, 22 s, −20 °C). The duration of the first SF_6 plasma step was 5 s only [82].

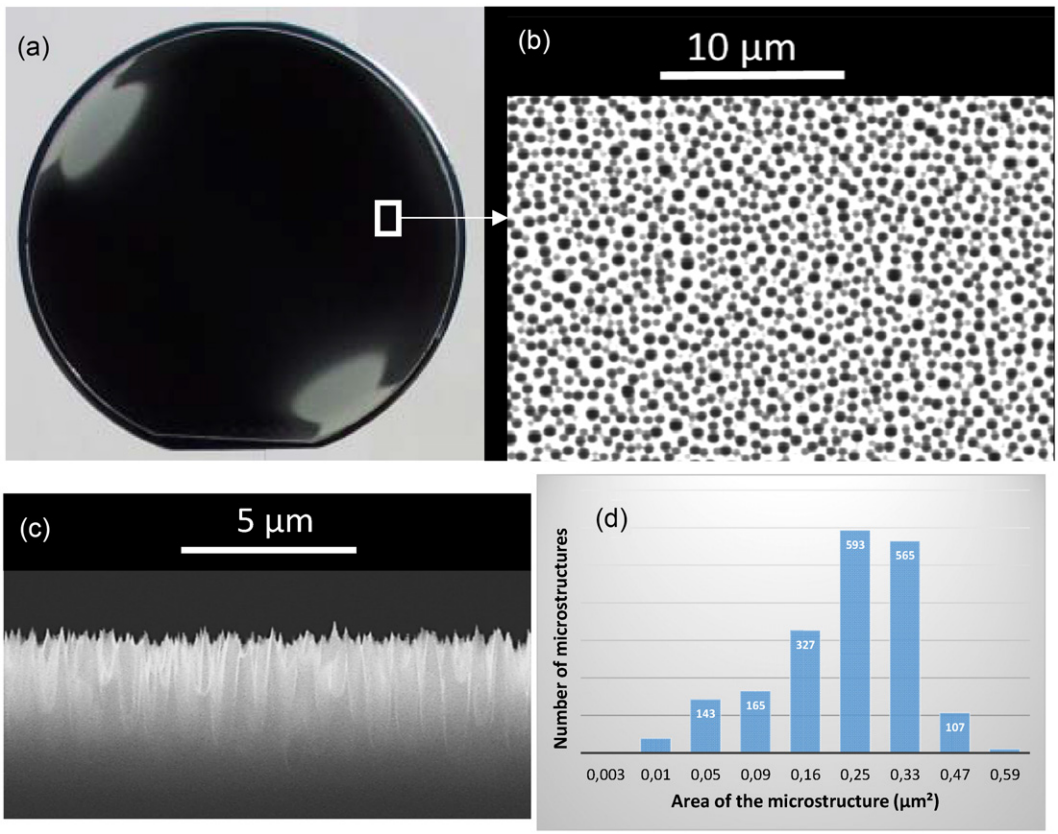

Figure 33. (*a*) Picture of 100 mm diameter wafer covered by black silicon after a cryoetching process; (*b*) SEM image of the CMS top view; (*c*) SEM image of the CMS side view; and, (*d*) Statistic on the CMS area using the SIMeG software.

a temperature between −30 and 0 °C. Dedicated double cavity experiments were carried out to study the formation of the SiO_xCl_y passivation and assess its resistance to SF_6 plasma [82]. 10 μm wide trenches were shallowly etched using such an alternating process (figure 32). Some tests on pulsed-mode $SF_6/SiCl_4$–$SiCl_4/O_2$ processes were also carried out and have enabled etch rates greater than 2 μm min^{-1} with a selectivity higher than 220 with SiO_2 masks. 2.5 μm and 5 μm wide trenches were successfully etched down to a depth of 20 μm and 25 μm, respectively, using this process. However, this process deposits some coating also on the reactor walls, which remains at ambient temperature and would require dedicated plasma cleaning steps to decontaminate the reactor wall from oxychloride layers.

5. Black silicon and CMS of silicon in cryoetching

5.1. Description of the phenomenon

As already mentioned, standard cryoetching can easily lead to the formation of grass at the bottom of the etched structures. This phenomenon is known as 'black-silicon' formation because the wafer parts covered by this type of microstructures appear black when enlightened (figure 33). This is usually obtained in over-passivating regime; that is, for a high content of oxygen in the plasma mixture. It is characterized by an oxidation threshold, as reported by Tillocher *et al* [45]. If SEM images are made in the black-silicon regions, one can observe quite organized CMSs. An example is given in figure 33.

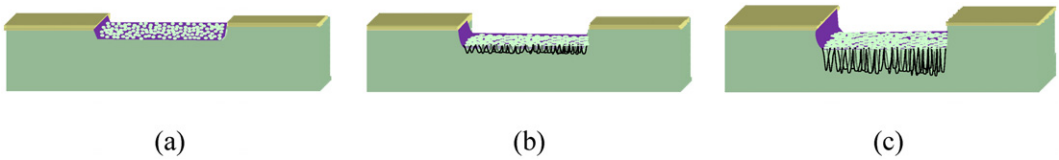

Figure 34. Schematic of grass formation in cryoetching: (*a*) initial roughness due to the etching–passivation competition; (*b*) formation of small cavities presenting vertical sidewalls and flat surfaces at the bottom; and, (*c*) accentuation and formation of nanostructures with an aspect ratio greater than one.

The dark areas in figure 33(*b*) represent the bottom of the microstructures. A dedicated software called SIMeG was made to accurately analyse the structures and make statistics on their dimensions [83]. The characteristic area of the CMS in this example is 0.3 μm^2, which corresponds to a typical diameter of 0.6 μm. The mean CMS height is 3.5 μm in this case (figure 33(*c*)). This structure was obtained after a 10 min long process, with a self-bias voltage of 20 V, a source power of 1000 W, a pressure of 3 Pa and a set-point temperature of −110 °C. CMS can be much deeper than those presented in figure 33. A typical height of 20–30 μm can be obtained by silicon cryoetching process.

Several papers dealing with black silicon for solar cell applications have been published [84–89]. Black silicon also has mechanical applications, such as those for the bonding processes [90]. Their ability to attach cells was also investigated [91]. Their capacity to convert light into heat and their efficiency as photo-thermal converters were also explored [92].

SF_6/O_2 ICP at non-cryogenic temperature can also induce black silicon (100 nm diameter and few micrometres deep columnar structures) at high oxygen content [93]. Bosch process in over-passivation regime can also lead to black-silicon formation [94]. Nanometric pattern transfer from organized nanodots formed on a polymeric film during etching was also successfully achieved [95].

Systematic studies of black-silicon formation in cryoetching have been carried out [29, 96, 97]. In particular, the appearance of black silicon has been used to develop the so-called 'black-silicon method'. This technique aims at defining a good recipe, providing a right balance between passivation and etching in order to provide vertical etched features [29].

The black-silicon formation mechanisms in cryogenic process are discussed in the next section.

5.2. Black-silicon mechanisms in cryogenic process

As mentioned in [96], in cryoetching, CMS only appear in over-passivating regimes; that is, for sufficient oxygen content, for a specific cryogenic temperature range and when both ion flux and energy are not too high. In this over-passivating regime, SiO_xF_y passivation layer growth dominates etching. The mechanisms responsible for black-silicon formation are schematically shown in figure 34. At the beginning of the plasma treatment, the surface is etched and some surface roughness appears due to the competition between etching and passivation. Shallow holes are first uniformly distributed and present a characteristic roughness dimension. It was demonstrated that an etched silicon surface can exhibit a network structure with holes which coarsen with etch time and a wavelength selection with a characteristic spatial frequency decreasing with time [98]. In cryoetching, the SiO_xF_y passivation layer forms preferentially on the more vertical sidewalls of the nanostructure hills, while the flat and horizontal surfaces of the valleys are etched by consuming fluorine radicals and provide SiF_4 molecules in the plasma. Step by step, structures with an aspect ratio greater than one appear. Roughness increases dramatically and black silicon is more and more pronounced. Black silicon corresponds to a sharp accentuation of the initial roughness generated at the beginning of the process. This mechanism of roughness accentuation is also suggested by Yang *et al* [93]. The authors also remind us that exothermic reactions of fluorine with silicon provides energy to the surface and reduces the probability of forming a new passivation layer at the bottom of the structures, as reported in [96].

As observed in figure 35, a residue from the passivation layer can be observed at the top of each microstructure. In figure 35(*a*), the passivation layer is still present at the top of formed nanopillars, whereas the passivation layer is only partially present on the top of the one shown in figure 35(*b*). For the nanopillar of figure 35(*b*), most of the passivation layer probably desorbed during the wafer warm-up to ambient temperature. However, in an over-passivating regime (i.e. for higher concentration of oxygen) the SiO_xF_y is probably richer in oxygen and more stable than the usual passivation layer, which forms in standard cryoetching conditions, so that some remaining SiO_xF_y material is still present at ambient temperature. This SiO_xF_y material can also be charged by ions and could slightly modify the ion trajectory, preventing their bombardment.

As already mentioned, SiF_x species can also help in forming the passivation layer and reinforce its robustness. As reported in [78], in SiF_4/O_2 plasma, some dust can be produced in the plasma. However, even if this dust could initiate some micromasking effect, dust redeposition and micromasking should not be the main mechanism responsible for the black-silicon formation, otherwise such organized structures would not appear on the surface. The fact that holes form with a characteristic size and are uniformly distributed indicates that the mechanism is more related to an accentuation of the initial roughness, which can lead to this type of organized structure. Moreover, as mentioned in [78], when dusts are formed in a plasma, they become negatively charged [99, 100] and are trapped above the sheath. They do not usually reach the surface until the plasma is switched off.

The parameter ranges in which CMS appear have been reported in a previous paper [96]. Figure 36 shows the regions

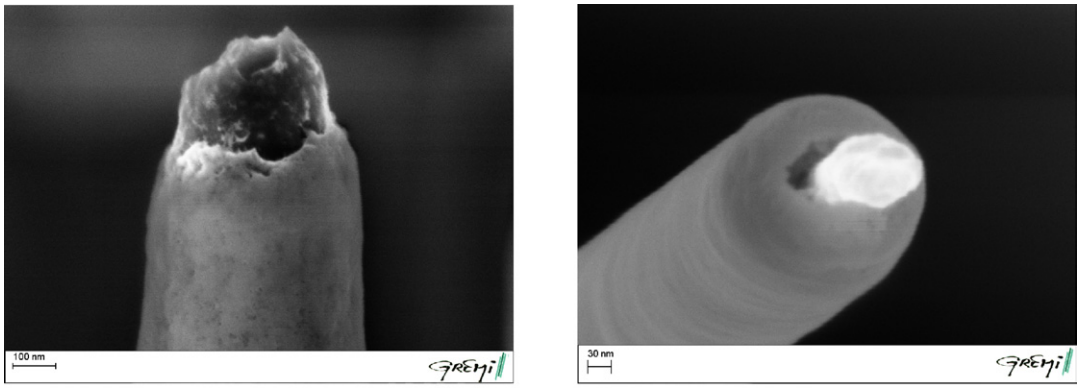

Figure 35. SEM images of the top of nanopillars formed in over-passivating regime and covered (*a*) completely or (*b*) partially by a remaining passivation material.

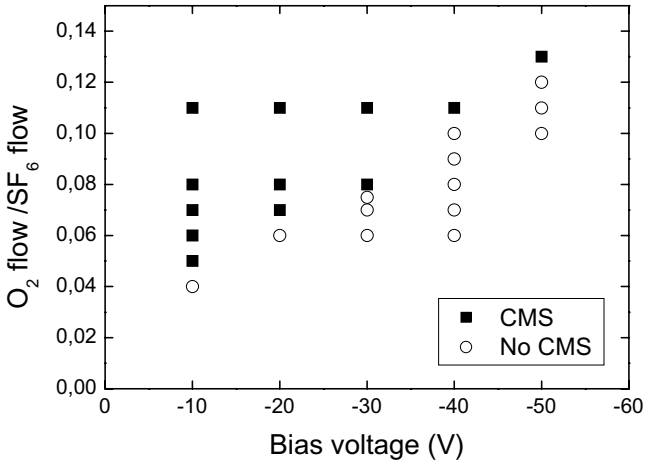

Figure 36. CMS formation zones versus O_2 content and bias voltage (power 1000 W, SF_6 flow = 200 sccm, $T = -110\,^{\circ}C$, pressure 3 Pa, 10 min) [96].

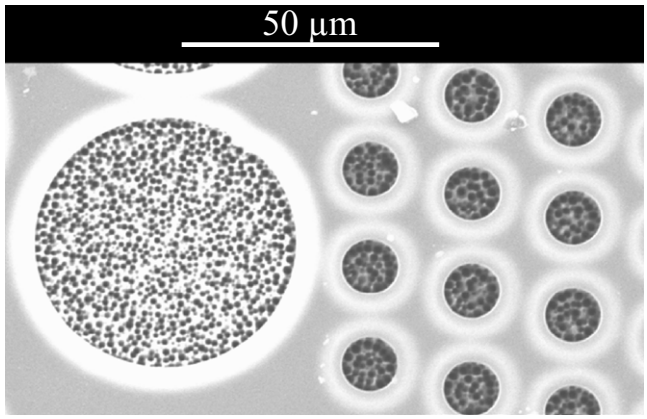

Figure 37. Micrograph of the top view of CMS obtained in an over-passivating regime in SF_6/O_2 plasma on a cooled ($-85\,^{\circ}C$) masked silicon wafer. CMS were observed in a 50 μm diameter hole and in 10 μm diameter holes. Reproduced with permission from [46]. Copyright 2007 Elsevier.

of CMS formation versus oxygen content and applied bias voltage. It is interesting to note that the boundary between the two regions of CMS formation and no CMS formation is a straight line. Ion energy increases linearly with self-bias voltage. So, we can assume that the crossing to the CMS formation actually corresponds to a threshold of energy density deposited at the surface, which switches the regime from over-passivation to etching. This is why it is important to consider chemical reactions at the surface and the silicon exposed area to the plasma. Exothermic reactions have to be taken into account in the total energy transfer to the substrate and are not negligible when the silicon area exposed to the plasma is quite large.

As reported in [46], the characteristic dimensions of black silicon can also depend on the pattern dimensions. This is illustrated in figure 37, where two CMS characteristic diameters can be observed on the SEM picture for two different diameters of hole pattern. The bigger CMS diameters are obtained in the smaller diameter hole patterns. This can be explained by etch by-products redeposition. SiF_x and O radicals could more easily reach the bottom of the structure in the 50 μm diameter hole because the aspect ratio is smaller in this case. Consequently, passivation mechanisms could be enhanced in the 50 μm diameter hole compared to the 10 μm diameter hole.

Experiments of CMS appearance were also carried out versus temperature [96]. By reducing the temperature from -110 to $-130\,^{\circ}C$ (figure 38), the morphology switches from holes to needles and the needle density decreases at very low temperature. If the temperature further decreases (e.g. $-140\,^{\circ}C$), then no black silicon is formed [96]. At a very low temperature, as mentioned previously, the crystallographic effect is more pronounced. This induces negative slopes of column sidewalls. When the sidewalls become too thin, the holes merge and needles instead of columns start to form.

CMS formation on narrow microstructures has also been investigated. In figure 39, the effect of CMS confinement in 10 and 5 μm wide trench structures is shown. In this case, CMS self-aligns in the trench.

Finally, we show that CMS and STiGer processes can be combined to achieve original structures, such as the micro-pillars shown in figure 40. In this particular process, a SF_6/O_2 plasma in over-passivating regime was first used to form the

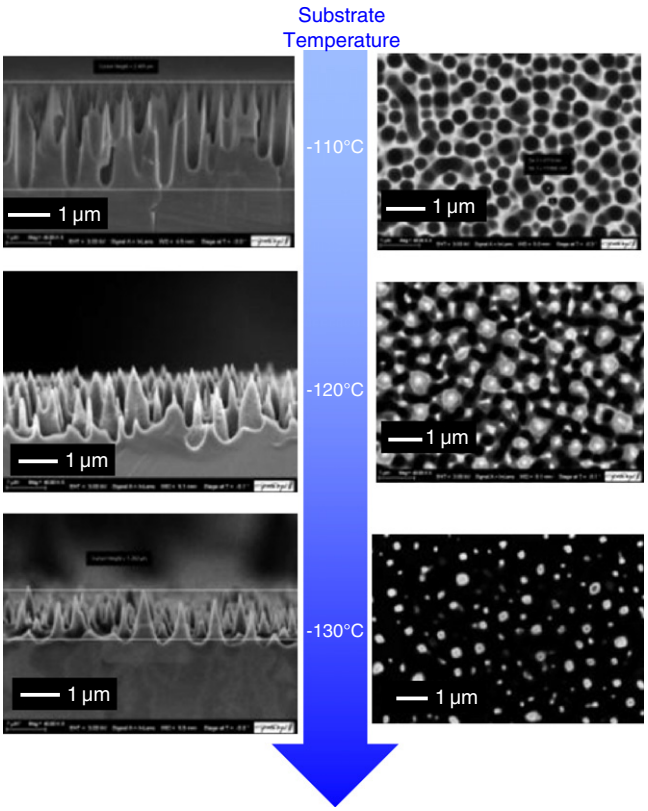

Figure 38. Evolution of CMS morphology versus temperature from −110 to −130 °C for the same process ($T = -110$ °C, $O_2/SF_6 = 0.12$, $p = 3$ Pa, $V_{bias} = -30$ V).

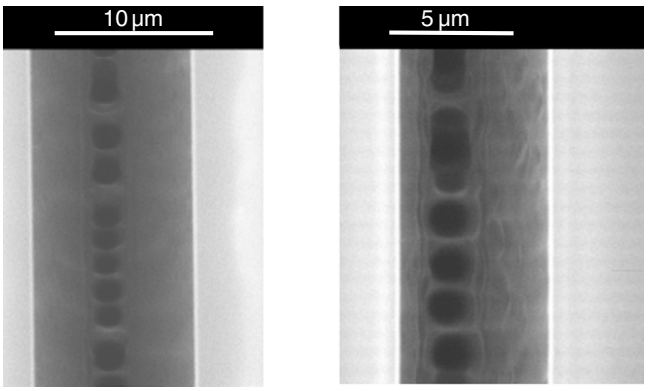

Figure 39. Self-alignment of CMS in 10 μm wide (a) and 5 μm wide (b) trenches.

initial CMS (100 sccm SF_6, 15 sccm O_2, $P_{source} = 1000$ W, Bias $= -20$ V, $P = 2.7$ Pa, $T = -120$ °C, 10 min). Then, a STiGer process was used to transfer the initial structure more deeply in the structure. (Etching steps: 200 sccm SF_6, 13 sccm O_2, $P_{source} = 1500$ W, Bias $= -50$ V, $P = 3.9$ Pa, $T = -83$ °C, 6 s; passivation steps: 50 sccm SiF_4, 20 sccm O_2, $P_{source} = 1500$ W, Bias$=-30$ V, $P = 1.3$ Pa, $T = -83$ °C, 3 s.) Micro-pillars as high as 40–50 μm were formed by this technique.

Note that another technique was successfully introduced by Sainiemi *et al* to form high-aspect-ratio silicon nanopillars by combining the liquid flame spray production of silica nanoparticle agglomerates with deep reactive ion cryoetching [101].

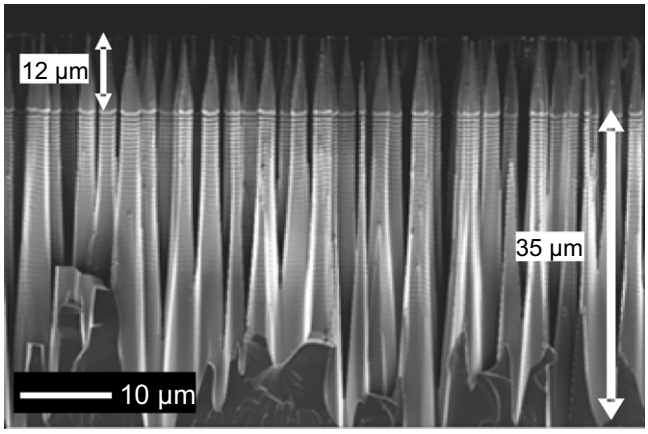

Figure 40. High-aspect-ratio structures obtained by forcing CMS formation using SF_6/O_2 plasma in an over-passivation regime during 10 min followed by a 10 min long STiGer process.

6. Cryoetching of silicon nanometric features and advanced processes for low-k materials

6.1. Nanometric features

It has recently been shown that cryogenic etching processes can also be used to etch 20 nm wide trenches [58], and even sub-10 nm features [59]. Figure 41 shows different trench sizes after 20 s etching. High selectivity with ZEP520A resist used for electron beam lithography with a mask thickness of around 60 nm has also been achieved. The etch rate of the resist is reduced by about 30% when the substrate temperature is −120 °C instead of 20 °C.

Another team has reported anisotropic etching of sub-15 nm silicon trenches from block copolymer templates using a standard cryoetching process [102]. Block copolymers are currently intensively studied for high resolution lithography [103]. In the experiments reported in [101], after solvent annealing and subsequent reconstruction in ethanol (figure 42(a)), an O_2/Ar RIE plasma mixture is first applied to obtain a polymeric line pattern consisting mainly of polystyrene (figure 42(b)). This step is then followed by a highly selective cryoetching process in SF_6/O_2 to transfer the polymer mask pattern onto the silicon substrate and form silicon trenches with an aspect ratio (figures 42(c) and (d)). An aspect ratio of about 5 has been obtained using this technique.

6.2. Advanced cryoetching processes of low-k materials

Low-k materials have been intensively studied and are used for back end of line (BEOL) technology applications. Porous organosilicate glasses (SiOCH) are currently the best candidates for interconnect applications [104]. One of the main challenges relies on the etching process since plasma-induced damage is quite critical for this material [105]. Several techniques have been suggested to pattern OSG by reducing plasma-induced damage. First, the 'post-integration porogen

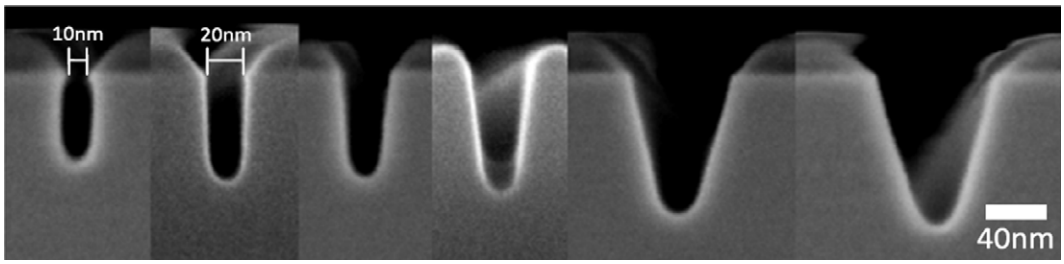

Figure 41. Si etching with $SF_6/O_2 = 34/16$ sccm, bias/ICP power = 5/1000 W, $P = 6$ mT, $T = -120\,^{\circ}$C. Different trench sizes after 20 s etching, 10, 20, 30, 40, 90, 110 nm from left to right [59].

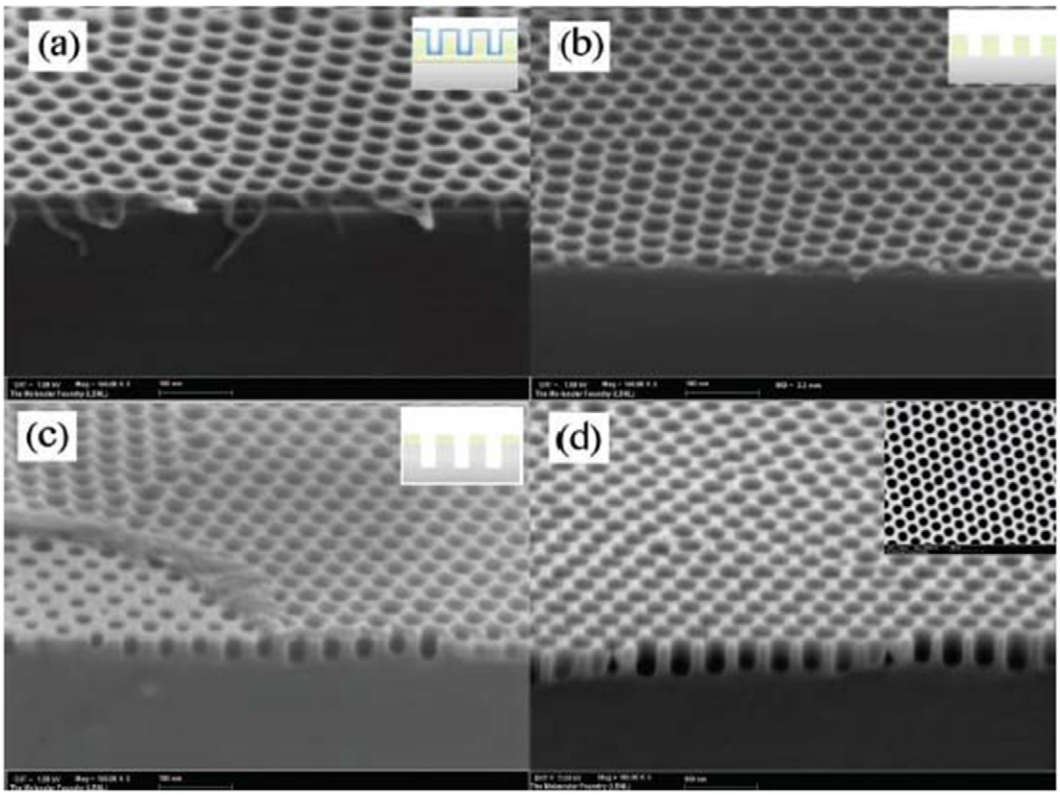

Figure 42. SEM images of a PS-b-PEO forming cylindrical domains oriented normal to the substrate. SEM was taken at a 60° tilt angle: (*a*) block copolymer pattern after solvent annealing and subsequent reconstruction in ethanol; (*b*) the film after an additional etching of 10 s in RIE; (*c*) transferred pattern in silicon after 10 s of cryo-ICP etching using the BCP mask; and, (*d*) silicon pattern after 20 s of cryo-ICP etching. Inset: image in (*d*) is the plane view of the silicon nanohole pattern. Reproduced with permission from [102]. Copyright 2012 Wiley.

removal' was proposed to use a hybrid material containing sacrificial porogens [106–108]). The 'post-porosity plasma protection-P4' approach uses a thermally degradable polymer to fill the porous structure of OSG dielectrics. Then, the material becomes dense (non-porous) and plasma-induced damage is reduced as the penetration of free radicals is blocked by the filled polymer [109, 110].

A low-*k* cryoetching approach has also been investigated [60, 61]. Since oxygen is already present in the composition of the material, cryoetching with just SF_6 plasma was first tested. Experiments were carried out on OSG-2.0 low-*k* material. The results are summarized in the graph of figure 43(*a*), where the etch rate of the film is plotted versus chuck temperature for two bias voltages. Etch rate is enhanced by ion bombardment and is reduced when substrate temperature is lowered. Without bias, etch rate reaches a plateau at a low temperature of between −80 and −120 °C. A process can be developed in this range of temperatures that could lead to an anisotropic profile since vertical walls, which are not submitted to ion bombardment, would not be etched by SF_6. The obtained profiles are shown in figure 43(*b*).

To make a comparison, we also show the profiles obtained in a $SiF_4/O_2/SF_6$ plasma at 20 °C after a 30 s long process. Note that a plasma with pure SF_6 on a sample at 20 °C leads to even worse profiles. The anisotropy is much improved at −120 °C with pure SF_6 plasma and plasma-induced damage is reduced in these conditions as reported in [61].

Other tests were performed by introducing SiF_4 and O_2 gases into a SF_6 plasma. The results are reported in [61]. In figure 44, a bar graph of the equivalent damaged layer (EDL)

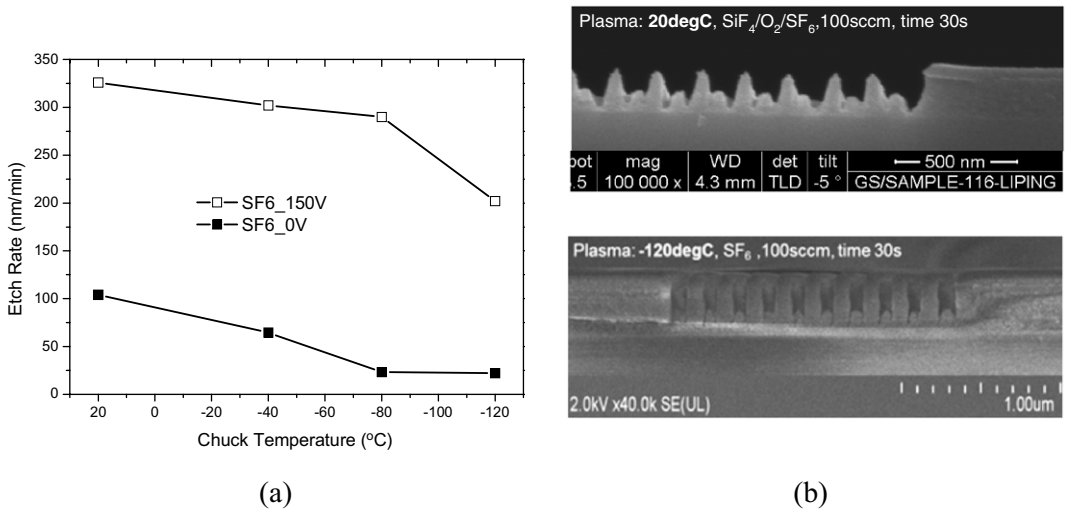

Figure 43. (*a*) Etching rate of OSG-2.0 in pure SF_6 plasma for two different bias powers versus chuck temperatures. Etching time=30 s, $P(SF_6) = 11.25$ mTorr, with ICP source power of 1000 W. (*b*) SEM pictures of the obtained profile on patterned wafers and at −120 °C after a 30 s long process. Reproduced with permission from [61]. Copyright 2013 The Electrochemical Society.

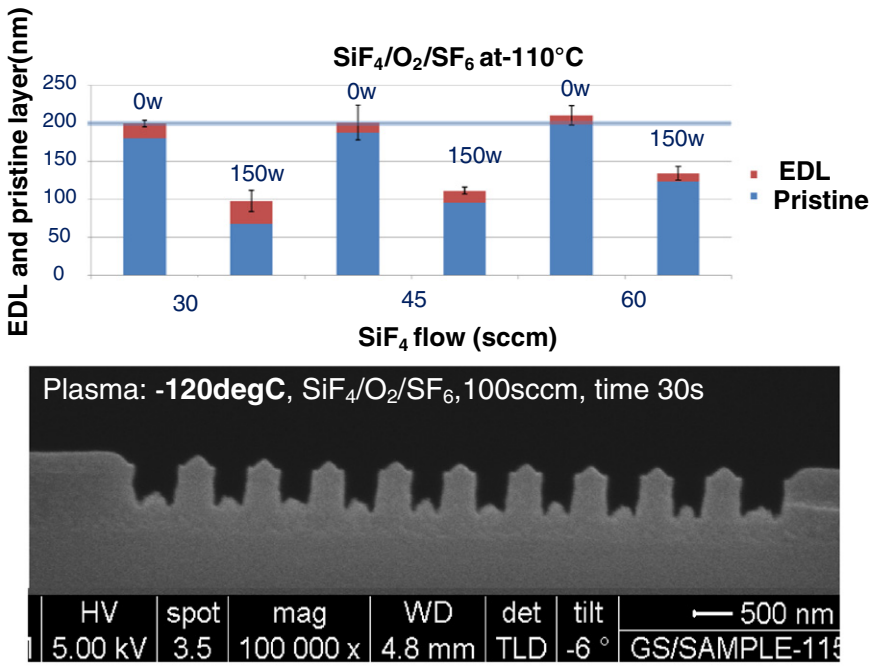

Figure 44. Top: equivalent damaged layer and pristine film of the porous SiOCH material after a 30 s long plasma treatment for three different SiF_4 flows, with (150 W) and without (0 W) bias at −110 °C. Below: SEM picture of trench profiles using such a process at −120 °C, 150 W bias with a SiF_4 flow of 60 sccm. Reproduced with permission from [61]. Copyright 2013 The Electrochemical Society.

and the pristine film is given for three different SiF_4 flows without (0 W) and with (150 W) bias. EDL is determined by FTIR and ellipsometry characterization. Promising results appear for 60 sccm of SiF_4 since no etch occurs at 0 W while etching is obtained at 150 W with a very low EDL and a quite reasonable sidewall roughness. The obtained profile is shown below the bargraph of figure 44.

As already explained in this paper, at cryogenic temperatures, SiO_xF_y can form or deposit at the surface. This property can be used to condense in the pores and block the penetration of active free radicals from the plasma. A part of this etch condensate can remain at room temperature, but can be easily removed by high-temperature annealing without additional damage to the low-*k* materials, as reported in [61]. Although the process has to be optimized to obtain a better trench profile and avoid the W shape at the bottom, cryoetching appears to be a quite promising technique for pourous SiOCH low-*k* etching.

7. General conclusions

During the 25 years after the first experiments on silicon cryoetching by Tachi's team, a number of involved physical and chemical mechanisms have been studied and partially understood by many teams. The main difficulty of these studies

relies on the fact that characterizations have to be carried out *in situ*. Very high-aspect-ratio silicon microstructures have been obtained by cryoetching using a wide variety of mask materials. Defects can be significantly reduced or eliminated by process optimization. One of the main characteristics of the cryoetching process is the almost complete desorption of the passivation layer after the etching process, just by warming the wafer back to ambient temperature. This can appear to be a significant advantage since micro- or nanostructures are clean and no longer covered by the passivation layer. Moreover, deposition only occurs on a cold surface and not on the reactor walls, which avoids plasma process drifts. Oxygen has to be injected in the SF_6 plasma to form the passivation layer at very low temperature of the substrate. Etch by-products (SiF_4) can participate in the passivation layer formation and reinforce it. SiF_x species can deposit on the sidewalls and react with oxygen radicals to form SiO_xF_y sites at the surface. When the wafer is warmed back to ambient temperature, the surface is modified: SiF_4 is formed and desorbs. These properties were inferred by different *in situ* characterization experiments (mass spectrometry, ellipsometry and XPS) and by double cavity test experiments. Cyclic processes have been proposed to enhance the robustness of the cryoetching process. Among them, the so-called STiGer process consists in alternating SiF_4/O_2 deposition plasmas with SF_6 etching plasmas. Process reproducibility is much enhanced using this particular process. The over-passivating regime at a higher oxygen content leads to the formation of black silicon or CMS at the surface of a blanket wafer. This self-organized microstructure can be used for dedicated applications where a large specific area has to be formed at the surface. In recent publications, it has been shown that sub-20 nm features could be successfully etched by the cryogenic process. Experiments have also been carried out using a mask of block copolymer. Finally, cryoetching is also of interest for porous SiOCH low-k etching without damaging the film. Pores can be filled with the passivation layer, which self-desorbs after the process so that plasma-induced damage is reduced.

Even if the understanding and control of the cryoetching process has been improved, some questions remain. For example, what is the stoichiometry of the passivation layer? What is the chemical mechanism in the formation of SiF_4 molecules when the wafer is warmed? And, what are the dimensional limits of the self-organized pattern obtained in an over-passivating regime? Research activity on cryoetching is still ongoing and may bring technical solutions to some current process limitations.

Acknowledgments

The authors would like to thank all of the collaborators who have contributed to the comprehension of the cryogenic etching, and in particular Pierre Ranson, Christophe Cardinaud, Grégory Marcos, Nasreddine Mekkakia, Mikhail Baklanov, Jean-François de Marneffe, Xavier Mellhaoui, Jérémy Péreira, El'Houcine Oubensaid, Julien Ladroue, Corinne Duluard, Hao Jiang, Vincent Girault, Liping Zhang, Bruneau Gary, Maite Volatier, Carole Socquet-Clerc and Wassim Kafrouni.

References

[1] Ramm P, Klumpp A, Weber J, Taklo M M V 2010 3D system-on-chip technologies for More than Moore systems *Microsyst. Technol.* **16** 1051
[2] Tachi S, Tsujimoto K and Okudaira S 1988 Low-temperature reactive ion etching and microwave plasma etching of silicon *Appl. Phys. Lett.* **52** 616
[3] Laermer F and Schilp A 1996 Method for anisotropic plasma etching of substrates *US Patent* 5498312 (assigned to Bosch GmbH)
[4] Poulsen R G 1977 Plasma etching in integrated circuit manufacture—a review *J. Vac. Sci. Technol.* **14** 266
[5] Jansen H V, Gardeniers H, de Boer M, Elwenspoek M and Fluitman J 1996 A survey on the reactive ion etching of silicon in microtechnology *J. Micromech. Microeng.* **6** 14
[6] Matsuo S 1980 Selective etching of Si relative to SiO_2 without undercutting by $CBrF_3$ plasma *Appl. Phys. Lett.* **36** 768
[7] Tachi S, Tsujimoto K, Arai S and Kure T 1991 Low-temperature dry etching *J. Vac. Sci. Technol.* A **9** 796
[8] Bestwick T D, Oehrlein G S and Angell D 1990 Cryogenic reactive ion etching of silicon in SF_6 *Appl. Phys. Lett.* **57** 431
[9] Tsujimoto K, Okudaira S and Tachi S 1991 Low-temperature microwave plasma etching of crystalline silicon *Japan. J. Appl. Phys.* **30** 3319
[10] Aydil E S, Gregus J A and Gottscho R A 1993 Electron cyclotron resonance plasma reactor for cryogenic etching *Rev. Sci. Instrum.* **64** 3572
[11] Bartha J W, Greschner J, Puech M and Maquin P 1995 Low temperature etching of Si in high-density plasma using SF_6/O_2 *Microelectron. Eng.* **27** 453
[12] Puech M and Maquin Ph 1996 Low temperature etching of Si and PR in high-density plasmas *Appl. Surf. Sci.* **100–101** 579
[13] Boswell R W and Porteous R K 1987 Large volume, high density rf inductively coupled plasma *Appl. Phys. Lett.* **50** 1130
[14] Perry A J and Boswell R W 1989 Fast anisotropic etching of silicon in an inductively coupled plasma reactor *Appl. Phys. Lett.* **55** 148
[15] d'Agostino R and Flamm D L 1981 Plasma etching of Si and SiO_2 in SF_6–O_2 mixtures *J. Appl. Phys.* **52** 162
[16] Oehrlein G S, Chan K K, Jaso M A, Rubloff G W 1989 Surface analysis of realistic semiconductor microstructures *J. Vac. Sci. Technol.* A **7** 1030
[17] Jansen H V, de Boer M J, Legtenberg R and Elwenspoek M C 1995 Black silicon method: I. A universal method for determining the parameter setting of a fluorine-based reactive ion etcher in deep silicon trench etching with profile control *J. Micromech. Microeng.* **5** 115
[18] Jansen H V, de Boer M J, Burger J, Legtenberg R and Elwenspoek M C 1995 Black silicon method: II. The effect of mask material and loading on the reactive ion etching of deep silicon trenches *Microelectron. Eng.* **27** 475
[19] Jansen H V, de Boer M J, Otter B and Elwenspoek M C 1995 The black silicon method: IV. The fabrication of three-dimensional structures in silicon with high aspect ratios for scanning probe microscopy and other applications *MEMS '95: Proc. IEEE Micro Electro Mechanical Systems (Amsterdam, Jan.–Feb. 1995)* p 88
[20] Esashi M, Takinami M, Wakabayashi Y and Minami K 1995 High-rate directional deep dry etching for bulk silicon micromachining *J. Micromech. Microeng.* **5** 5
[21] Wells T, El-Gomati M M and Wood J 1997 Low temperature reactive ion etching of silicon with SF_6/O_2 plasmas *J. Vac. Sci. Technol.* B **15** 434
[22] Chevolleau T, Tessier P Y, Cardinaud C and Turban G 1997 Etching of Si at low temperatures using a SF_6 reactive ion

beam: effect of the ion energy and current density *J. Vac. Sci. Technol.* A **15** 2661
[23] Tessier P Y, Chevolleau T, Cardinaud C and Grolleau B 1999 An XPS study of the SF_6 reactive ion beam etching of silicon at low temperatures *Nucl. Instrum. Methods Phys. Res.* B **155** 280
[24] Oehrlein G S and Kurogi Y 1998 Sidewall surface chemistry in directional etching processes *Mater. Sci. Eng.* **24** 153
[25] Aachboun S and Ranson P 1999 Deep anisotropic etching of silicon *J. Vac. Sci. Technol.* A **17** 2270
[26] Aachboun S, Ranson P, Hilbert C and Boufnichel M 2000 Cryogenic etching of deep narrow trenches in silicon *J. Vac. Sci. Technol.* A **18** 1848
[27] Zijlstra T and van der Drift E 1999 Fabrication of two-dimensional photonic crystal wave guides for 1.5 um in silicon by deep anisotropic dry etching *J. Vac. Sci. Technol.* B **17** 2734
[28] Blauw M A, Zijlstra T, Bakker R A and van der Drift E 2000 Kinetics and crystal orientation dependence in high aspect ratio silicon dry etching *J. Vac. Sci. Technol.* B **18** 3453
[29] Jansen H V, de Boer M J, Wensink H, Kloeck B and Elwenspoek M C 2001 Black silicon method: VIII. A study of the performance of etching silicon using SF_6/O_2-based chemistry with cryogenical wafer cooling and a high-density ICP source *Microelectron. J.* **32** 769
[30] de Boer M J, Gardeniers J G E, Jansen H V, Smulders E, Gilde M-J, Roelofs G, Sasserath J N and Elwenspoek M C 2002 Black silicon method: IX. Guidelines for etching silicon MEMS structures using fluorine high-density plasmas at cryogenic temperatures *J. Microelectromech. Syst.* **11** 385
[31] Boufnichel M, Aachboun S, Grangeon F, Lefaucheux P and Ranson P 2002 Profile control of high aspect ratio trenches of silicon: I. Effect of process parameters on local bowing *J. Vac. Sci. Technol.* B **20** 1508
[32] Boufnichel M, Aachboun S, Lefaucheux P and Ranson P 2003 Profile control of high aspect ratio trenches of silicon: II. Study of the mechanisms responsible for local bowing formation and elimination of this effect *J. Vac. Sci. Technol.* B **21** 267
[33] Boufnichel M, Lefaucheux P, Aachboun S, Dussart R and Ranson P 2005 Origin, control and elimination of undercut in silicon deep plasma etching in the cryogenic process *Microelectron. Eng.* **77** 327
[34] Marcos G, Rhallabi A and Ranson P 2003 Monte Carlo simulation method for etching of deep trenches in Si by a SF_6/O_2 plasma mixture *J. Vac. Sci. Technol.* B **21** 87
[35] Blauw M A, van der Drift E, Marcos G and Rhallabi A 2003 Modeling of fluorine-based high-density plasma etching of anisotropic silicon trenches with oxygen sidewall passivation *J. Appl. Phys.* **94** 6311
[36] Marcos G, Rhallabi A and Ranson P 2004 Topographic and kinetic effects of the SF_6/O_2 rate during a cryogenic etching process of silicon *J. Vac. Sci. Technol.* B **22** 1912
[37] Kokkoris G, Gogolides E, Boudouvis A G 2002 Etching of SiO_2 features in fluorocarbon plasmas: explanation and prediction of gas-phase-composition effects on aspect ratio dependent phenomena in trenches *J. Appl. Phys.* **91** 2697
[38] Knizikevicius R 2002 Evaluation of desorption activation energy of SiF_4 molecules *Vacuum* **68** 29
[39] Knizikevicius R and Kopustinskas V 2004 Anisotropic etching of silicon in SF_6 plasma *Vacuum* **77** 1
[40] Knizikevicius R 2006 Simulation of anisotropic etching of silicon in SF_6+O_2 plasma *Sensors Actuators* A **132** 726
[41] Maruyama T, Narukage T, Onuki R and Fujiwara N 2010 High-aspect-ratio deep Si etching in SF_6/O_2 plasma: I. Characteristics of radical reactions with high-aspect-ratio patterns *J. Vac. Sci. Technol.* B **28** 854
[42] Rangelow I W 2003 Critical tasks in high aspect ratio silicon dry etching for MEMS *J. Vac. Sci. Technol.* A **21** 1550
[43] Dussart R, Boufnichel M, Marcos G, Lefaucheux P, Basillais A, Benoit R, Tillocher T, Mellhaoui X, Estrade-Szwarckopf H and Ranson P 2004 Passivation mechanisms in cryogenic SF_6/O_2 etching process *J. Micromech. Microeng.* **14** 190
[44] Mellhaoui X, Dussart R, Tillocher T, Lefaucheux P, Ranson P, Boufnichel M and Overzet L J 2005 SiO_xF_y passivation layer in silicon cryoetching *J. Appl. Phys.* **98** 104901
[45] Tillocher T, Dussart R, Mellhaoui X, Lefaucheux P, Mekkakia Maaza N, Ranson P, Boufnichel M and Overzet L J 2006 Oxidation threshold in silicon etching at cryogenic temperatures *J. Vac. Sci. Technol.* A **24** 1073
[46] Dussart R, Mellhaoui X, Tillocher T, Lefaucheux P, Boufnichel M and Ranson P 2007 The passivation layer formation in the cryo-etching plasma process *Microelectron. Eng.* **84** 1128
[47] Duluard C Y, Dussart R, Tillocher T, Pichon L E, Lefaucheux P, Puech M and Ranson P 2008 SO_2 passivating chemistry for silicon cryogenic deep etching *Plasma Sources Sci. Technol.* **17** 045008
[48] Pereira J, Pichon L E, Dussart R, Cardinaud C, Duluard C Y, Oubensaid E H, Lefaucheux P, Boufnichel M and Ranson P 2009 *In situ* x-ray photoelectron spectroscopy analysis of SiO_xF_y passivation layer obtained in a SF_6/O_2 cryoetching process *Appl. Phys. Lett.* **94** 071501
[49] Sainiemi L and Franssila S 2007 Mask material effects in cryogenic deep reactive ion etching *J. Vac. Sci. Technol.* B **25** 801
[50] Pruessner M W, Rabinovich W S, Stievater T H, Park D and Baldwin J W 2007 Cryogenic etch process development for profile control of high aspect-ratio submicron silicon trenches *J. Vac. Sci. Technol.* B **25** 21
[51] Tillocher T, Dussart R, Overzet L J, Mellhaoui X, Lefaucheux P, Boufnichel M and Ranson P 2008 Two cryogenic processes involving SF_6, O_2, and SiF_4 for deep etching *J. Electrochem. Soc.* **155** D187
[52] Dussart R, Tillocher T, Lefaucheux P, Ranson P, Mellhaoui X, Boufnichel M and Overzet L J 2008 Deep anisotropic silicon etch method *France Patent* 2914782-A1 (assigned to STMicroelectronics, CNRS and University of Orleans)
[53] Isakovic A F, Evans-Lutterodt K, Elliott D, Stein A and Warren J B 2008 Cyclic, cryogenic, highly anisotropic plasma etching of silicon using SF_6/O_2 *J. Vac. Sci. Technol.* A **26** 1182
[54] Jansen H V, de Boer M J, Unnikrishnan S, Louwerse M C and Elwenspoek M C 2009 Black silicon method X: a review on high speed and selective plasma etching of silicon with profile control: an in-depth comparison between Bosch and cryostat DRIE processes as a roadmap to next generation equipment *J. Micromech. Microeng.* **19** 033001
[55] Henry M D, Welch C and Scherer A 2009 Techniques of cryogenic reactive ion etching in silicon for fabrication of sensors *J. Vac. Sci. Technol.* A **27** 1211
[56] Sökmen Ü, Stranz A, Fünding S, Merzsch S, Neumann R, Wehmann H H, Peiner E and Waag A 2010 Shallow and deep dry etching of silicon using ICP cryogenic reactive ion etching process *Microsyst. Technol.* **16** 863
[57] Kamto A, Divan R, Sumant A V and Burkett S L 2010 Cryogenic inductively coupled plasma etching for fabrication of tapered through-silicon vias *J. Vac. Sci. Technol.* A **28** 719
[58] Wu Y, Olynick D L, Goodyear A, Peroz C, Dhuey S, Liang X and Cabrini S 2011 Cryogenic etching of nano-scale silicon trenches with resist masks *Microelectron. Eng.* **88** 2785
[59] Liu Z, Wu Y, Harteneck B and Olynick D 2013 Super-selective cryogenic etching for sub-10 nm features *Nanotechnology* **24** 015305

[60] Zhang L, Ljazouli R, Lefaucheux P, Tillocher T, Dussart R, Mankelevich Y A, de Marneffe J F, de Gendt S and Baklanov M R 2013 Damage free cryogenic etching of a porous organosilica ultralow-*k* film *ECS Solid State Lett.* **2** N5

[61] Zhang L, Ljazouli R, Lefaucheux P, Tillocher T, Dussart R, Mankelevich Y A, de Marneffe J F, de Gendt S and Baklanov M R 2013 Low damage cryogenic etching of porous organosilicate low-*k* materials using $SF_6/O_2/SiF_4$ *ECS J. Solid State Sci. Technol.* **2** 131

[62] Hibert C, Aachboun S, Boufnichel M and Ranson P 2001 Study of a mechanically clamped cryo-chuck device in a high-density plasma for deep anisotropic etching of silicon *J. Vac. Sci. Technol.* A **19** 646

[63] Lieberman M A and Lichtenberg A J 1994 *Principles of Plasma Discharges and Processing* (New York: Wiley)

[64] Gomez S, Belen R J, Kiehlbauch M and Aydil E S 2004 Etching of high aspect ratio structures in Si using SF_6/O_2 plasma *J. Vac. Sci. Technol.* A **22** 606

[65] Gomez S, Belen R J, Kiehlbauch M and Aydil E S 2005 Etching of high aspect ratio features in Si using SF_6/O_2/HBr and $SF_6/O_2/Cl_2$ plasma *J. Vac. Sci. Technol.* A **23** 1592

[66] Walker M J 2001 Comparison of Bosch and cryogenic processes for patterning high aspect ratio features in silicon *Proc. SPIE* **4407** 89

[67] Dussart R, Thomann A L, Pichon L E, Bedra L, Semmar N, Lefaucheux P, Mathias J and Tessier Y 2008 Direct measurements of the energy flux due to chemical reactions at the surface of a silicon sample interacting with a SF_6 plasma *Appl. Phys. Lett.* **93** 131502

[68] Oubensaid E H, Duluard C Y, Pichon L E, Morillon B, Boufnichel M, Lefaucheux P, Dussart R and Ranson P 2009 Cryogenic etching of n-type silicon with p+ doped walls with the TGZM process through the Al/Si eutectic alloy *Microelectron. Eng.* **86** 2262

[69] Tillocher T, Dussart R, Mellhaoui X, Lefaucheux P, Boufnichel M and Ranson P 2007 Silicon cryo-etching of deep holes *Microelectron. Eng.* **84** 1120

[70] Maruyama T, Narukage T, Onuki R and Fujiwara N 2010 High-aspect-ratio deep Si etching in SF_6/O_2 plasma: II. Mechanism of lateral etching in high-aspect-ratio features *J. Vac. Sci. Technol.* B **28** 862

[71] Craciun G, Blauw M A, van der Drift E, Sarro P M and French P J 2002 Temperature influence on etching deep holes with SF_6/O_2 cryogenic plasma *J. Micromech. Microeng.* **12** 390

[72] Ligenza J R 1961 Effect of crystal orientation on oxidation rates of silicon in high pressure steam *J. Phys. Chem.* **65** 2011

[73] Mekkakia-Maaza N, Dussart R, Tillocher T, Lefaucheux P and Ranson P 2013 A novel amorphization-etch alternating process for Si(1 0 0) *J. Micromech. Microeng.* **23** 045023

[74] Zhang J and Fisher E R 2004 Creation of SiOF films with SiF_4/O_2 plasmas: from gas–surface interactions to film formation *J. Appl. Phys.* **96** 1094

[75] Kim J H, Seo S H, Yun S M, Changa H Y, Lee K M and Choi C K 1996 The deposition of SiOF film with low dielectric constant in a helicon plasma source *Appl. Phys. Lett.* **68** 1507

[76] Lee S and Park J W 1996 Effect of fluorine on dielectric properties of SiOF films *J. Appl. Phys.* **80** 5260

[77] Kim S P and Choi S K 2000 The origin of intrinsic stress and its relaxation for SiOF thin films deposited by electron cyclotron resonance plasma-enhanced chemical vapor deposition *Thin Solid Films* **379** 259

[78] Jansen H V, de Boer M J, Ma K, Gironès M, Unnikrishnan S, Louwerse M C and Elwenspoek M C 2010 Black silicon method XI: oxygen pulses in SF_6 plasma *J. Micromech. Microeng.* **20** 075027

[79] Tillocher T, Kafrouni W, Ladroue J, Lefaucheux P, Boufnichel M, Ranson P and Dussart R 2011 Optimization of submicron deep trench profiles with the STiGer cryoetching process: reduction of defects *J. Micromech. Microeng.* **21** 085005

[80] Defforge T, Songa X, Gautier G, Tillocher T, Dussart R, Kouassi S and Tran-Van F 2011 Scalloping removal on DRIE via using low concentrated alkaline solutions at low temperature *Sensors Actuators* A **170** 114

[81] Duluard C Y, Ranson P, Pichon L E, Oubensaid E H, Pereira J, Lefaucheux P, Puech M and Dussart R 2009 Neutral species in inductively coupled $SF_6/SiCl_4$ plasmas *J. Phys. D: Appl. Phys.* **42** 115206

[82] Duluard C Y, Ranson P, Pichon L E, Pereira J, Oubensaid E H, Lefaucheux P, Puech M and Dussart R 2011 Alternating $SiCl_4/O_2$ passivation steps with SF_6 etch steps for silicon deep etching *J. Micromech. Microeng.* **21** 065015

[83] Bruneau G 2002 *SIMEG Software, ESPEO-Polytech* (Orléans: Université d'Orléans)

[84] Yoo J S, Parm I O, Gangopadhyay U, Kim K, Dhungel S K, Mangalaraj D and Yi J 2006 Black silicon layer formation for application in solar cells *Sol. Energy Mater. Sol. Cells* **90** 3085

[85] Yoo J, Kim K, Thamilselvan M, Lakshminarayn N, Kim Y K, Lee J, Yoo K J and Yi J 2008 RIE texturing optimization for thin c-Si solar cells in SF_6/O_2 plasma *J. Phys. D: Appl. Phys.* **41** 125205

[86] Yoo J, Yua G and Yi J 2009 Black surface structures for crystalline silicon solar cells *Mater. Sci. Eng.* B **159** 333

[87] Branz H M, Yost V E, Ward S, Jones K M, To B and Stradins P 2009 Nanostructured black silicon and the optical reflectance of graded-density surfaces *Appl. Phys. Lett.* **94** 231121

[88] Iyengar V V, Nayak B K and Gupta M C 2010 Optical properties of silicon light trapping structures for photovoltaics *Sol. Energy Mater. Sol. Cells* **94** 2251

[89] Xia Y, Liu B, Liu J, Shen Z and Li C 2011 A novel method to produce black silicon for solar cells *Sol. Energy* **85** 1574

[90] Stubenrauch M, Fischer M, Kremin C, Stoebenau S, Albrecht A and Nagel O 2006 Black silicon—new functionalities in microsystems *J. Micromech. Microeng.* **16** S82

[91] Turner S, Kam L Isaacson M, Craighead H G, Shain W and Turner J J 1997 Cell attachment on silicon nanostructures *Vac. Sci. Technol.* B **15** 2848

[92] Nguyen K N, Abi-Saab D, Basset P, Richalot E, Malak M, Pavy N, Flourens F, Marty F, Angelescu D, Leprince-Wang Y and Bourouina T 2012 Study of black silicon obtained by cryogenic plasma etching: approach to achieve the hot spot of a thermoelectric energy harvester *Microsyst. Technol.* **18** 1807

[93] Yang C, Ryu S-H, LIM Y-D and Yoo W J 2008 Self-assembly of Si nanostructures in SF_6/O_2 plasma *Nano* **3** 169

[94] Leopold S, Kremin C, Ulbrich A, Krischok S and Hoffmann M 2011 Formation of silicon grass: nanomasking by carbon clusters in cyclic deep reactive ion etching *J. Vac. Sci. Technol.* B **29** 011002

[95] Vourdas N, Kontziampasis D, Kokkoris G, Constantoudis V, Goodyear A, Tserepi A, Cooke M and Gogolides E 2010 Plasma directed assembly and organization: bottom-up nanopatterning using top-down technology *Nanotechnology* **21** 085302

[96] Dussart R, Mellhaoui X, Tillocher T, Lefaucheux P, Volatier M, Socquet-Clerc C, Brault P and Ranson P 2005 Silicon columnar microstructures induced by an SF_6/O_2 plasma *J. Phys. D: Appl. Phys.* **38** 3395

[97] Nguyen K N, Basset P, Marty F, Leprince-Wang Y and Bourouina T 2013 On the optical and morphological properties of microstructured black silicon obtained by cryogenic-enhanced plasma reactive ion etching *J. Appl. Phys.* **113** 194903
[98] Zhao Y P, Drotar J T, Wang G C and Lu T M 1999 Roughening in plasma etch fronts of Si(1 0 0) *Phys. Rev. Lett.* **82** 4882
[99] Couëdel L, Mikikian M, Boufendi L and Samarian A A 2006 Residual dust charges in discharge afterglow *Phys. Rev.* E **74** 026403
[100] Boufendi L, Jouanny M Ch, Kovacevic E, Berndt J and Mikikian M 2011 Dusty plasma for nanotechnology *J. Phys. D: Appl. Phys.* **44** 174035
[101] Sainiemi L, Keskinen H, Aromaa M, Luosujärvi L, Grigoras K, Kotiaho T, Mäkelä J M and Franssila S 2007 Rapid fabrication of high aspect ratio silicon nanopillars for chemical analysis *Nanotechnology* **18** 505303
[102] Gu X, Liu Z, Gunkel I, Chourou S T, Hong S W, Olynick D L and Russell T P 2012 High aspect ratio sub-15 nm silicon trenches from block copolymer templates *Adv. Mater.* **24** 5688
[103] Sinturel C, Vayer M, Morris M and Hillmyer M A 2013 Solvent vapor annealing of block polymer thin films *Macromolecules* **46** 5399
[104] Dubois G and Volksen W 2012 Low-*k* materials: recent advances *Advanced Interconnects for ULSI Technology* ed M R Baklanov *et al* (Chichester: Wiley)
[105] Darnon M *et al* 2013 Impact of low-*k* structure and porosity on etch processes *J. Vac. Sci. Technol.* B **31** 011207
[106] Calvert J M and Gallagher M K 2003 A new approach to ultralow-*k* dielectrics *Semicond. Int.* **26** 56
[107] Jousseaume V, Favennec L, Zenasni A and Passemard G 2006 Plasma-enhanced chemical-vapor-deposited ultralow *k* for a postintegration porogen removal approach *Appl. Phys. Lett.* **88** 182908
[108] Fayolle M *et al* 2004 Cu/ULK integration using a post integration porogen removal approach *Proc. IEEE Int. Interconnect Technology Conf. (Burlingame, CA, June 2004)* p 208
[109] Frot T, Volksen W, Purushothaman S, Bruce R and Dubois G 2011 Application of the protection/deprotection strategy to the science of porous materials *Adv. Mater.* **23** 2828
[110] Frot T, Volksen W, Purushothaman S, Bruce R L, Magbitang T, Miller D C, Deline V R and Dubois G 2012 Post porosity plasma protection: scaling of efficiency with porosity *Adv. Funct. Mater.* **22** 3043